3AB

DAEDALEAN ASSOCIATES, Incorporated

TECHNICAL REPORT

TECHNICAL REPORT ON THE LABORATORY APPLICATION OF A NONDESTRUCTIVE EVALUATION TECHNIQUE FOR DETECTING INCIPIENT CRACK FORMATION IN MODEL OFFSHORE STRUCTURES

Prepared for:

Office of Naval Research
Department of the Navy
Structural Mechanics Program
Code 474
Arlington, Virginia 22217

by

B. Jachowski,

D. C. Fresch,

R. G. Brasfield,

and

A. P. Thiruvengadam

DAI Technical Report
LLY-7763-003-TR

May 1980

CREDITS AND ACKNOWLEDGMENTS

This report has been prepared under the auspices of the Material Systems Division of the Springlake Research Center of DAEDALEAN ASSOCIATES, Incorporated.

Dr. A. P. Thiruvengadam was the Principal Investigator. Mr. Larry Yeager is the Technical Director and Mr. Ray G. Brasfield is the Department Head of the Material Systems Division. Mr. Bruce Jachowski was the Project Engineer. The 1/14 scale model structure was initially designed and fabricated by Mr. Frederick Franz. Mr. Franz was also responsible for the design and construction of the electrohydraulic loading device.

The authors wish to acknowledge Gulf Oil Company for providing background information on offshore structures.

The authors also wish to acknowledge the co-sponsors: Mr. John Gregory, Program Manager for the Research and Development Program for Outer Continental Shelf Oil and Gas Operations, U. S. Geological Survey; and Dr. Nicholas Perrone, Program Manager for the Structural Mechanics Program, Office of Naval Research.

ABSTRACT

This report discusses the technical feasibility of applying an Internal Friction Damping - Nondestructive Evaluation technique for offshore structures. The theory of internal friction damping is presented as it has been historically applied to various materials. The report then discusses the methodology for the application of internal friction damping. The experimental apparatus and specific laboratory technique as applied to a 1/14 scale model offshore structure is next discussed in detail. The experimental test results are related to the feasibility of employing the test technique as a device for detecting incipient cracking in offshore structures. The report includes discussion of specific conclusions and recommendations for further investigation of in-service offshore structures.

TABLE OF CONTENTS

Page

Page

Page

LIST OF TABLES AND FIGURES

TECHNICAL REPORT ON THE LABORATORY APPLICATION OF A NONDESTRUCTIVE EVALUATION TECHNIQUE FOR DETECTING INCIPIENT CRACK FORMATION IN MODEL OFFSHORE STRUCTURES

1.0 INTRODUCTION

Tower structures have been used in many diverse engineering applications. Their weight versus strength allows them to be used in many instances where simple supports would not be appropriate. This century has seen the tower structure applications extend to offshore areas. In the United States, these offshore structures have been used for radar stations, lighthouses, weather stations and oil and gas drilling platform supports (1)*. The corrosive environment of the oceans, together with wind, wave and current forces can accelerate material degradation of tower structures and lead to subsequent material failures.

Concern for the safety of both the older structures, nearing the end of the calculated design life, and the newer and future structures, has increased. The development of nondestructive evaluation techniques to monitor the condition of offshore structures would be clearly desirable.

In order to evaluate the application of the Internal Friction Damping - Nondestructive Evaluation (IFD-NDE) technique to

* Numbers in parentheses refer to references at the end of this report.

offshore structures, a three phase program was initiated by the U. S. Geological Survey (USGS) and the Office of Naval Research (ONR). The first phase consisted of two parts: 1) a preliminary investigation of the feasibility of applying the IFD-NDE technique to a model offshore structure (2), and 2) a follow-on program to determine the feasibility of the IFD-NDE technique to determine a structural degradation and member cracking in the model tower structure. This technical report addresses the work done in the second part of Phase I.

The inspection technique measures the internal friction damping (IFD) of the material during its work cycle history. Specifically, the internal friction damping is measured as a function of time in-service in order to detect a change in the dynamic response of the structure material. Laboratory data from a 1/14 scale model tower was generated in order to evaluate the applicability of this technique as a surveillance procedure for offshore tower structures. This technical report identifies the salient results, conclusions and recommendations as a culmination of the work performed in the laboratory program.

1.1 Background on Tower Structures, Inspection Methods and the IFD-NDE Application History

Offshore tower structures vary in design and materials depending upon application and expected load history. Also, these structures are exposed to various environments which aid and accelerate particular failure modes.

Many early offshore structures stemmed from the development required for military applications. The mobile wharf developed by Delong Engineering and Construction Company is such a structure. This device consists of a barge-like deck with holes for cylindrical steel columns. Details of this construction method can be found in Reference (1) and will not be covered here. The Delong mobile wharf was used for radar towers and lighthouse applications. Its popularity stemmed from its speed and ease of assembly compared to the standard construction techniques.

The first offshore oil drilling platform was constructed in 1911 at Cadds Lake, Louisiana. It was constructed of wood and consisted of wooden piles topped by a platform. Oil exploration began in Lake Maracaibo, Venezuela in 1925 also using wooden piling platform design rigs. However, this wood soon fell prey to marine borers and had to be replaced. Precast concrete piles were substituted and have been the primary construction material since. Steel was not used because of the highly corrosive nature of the water in the lake.

Gulf of Mexico, Atlantic and Pacific coastal water drilling has seen the use of a steel-template design. These structures are of truss-design type and are "pinned" to the ocean floor by means of piles driven through the tubular support columns of the structure. After the piles are driven, the structure is then welded to the pilings. A similar truss

design type is simply called the "tower" type. It is usually floated and towed out to the site and lowered by progressive flooding. It may or may not be anchored by pilings.

Seawater is a fairly uniform solution of sodium and magnesium chlorides with other trace minerals. The high chloride concentration combined with dissolved oxygen creates a very corrosive environment for structural carbon steels. Exposed steel in seawater has a corrosion rate of 2 to 5 mils per year (3). The rate of corrosion is higher in the tropics than in cold water areas and is also higher in zones of high dissolved oxygen content. High velocity currents tend to accelerate corrosion by erosion of the oxide coating. Corrosion of steel in seawater is an electrolytic reaction where slight differences in electronegativity between adjacent areas of the surface permit galvanic action to occur. Corrosion protection for offshore steel structures usually includes organic coatings and cathodic protection.

Combination of the effects of corrosion and fatigue stresses induced by wind, wave and current forces can result in structural failures. Current inspection methods are discussed in the following section.

1.1.1 Current Inspection Methods

Various inspections are conducted during both construction and use of offshore tower structures. In the construction phase, visual, radiographic, magnetic particle and/or

ultrasonic testing techniques are used. Weld inspection by radiography must follow AWS D1.1 Sections 8.15.2 (buildings) or 10.17.2 (tubular structures) standards. Magnetic particle inspection must follow ASTM E 109-63. During the life of an offshore structure, periodic surveys are conducted to detect any evidence of damage and to monitor the adequacy of the corrosion protection system. Primary method for this in-service inspection is visual examination of the structure in the above water, air/water interface (splash) and below water zones. Spot ultrasonic or radiographic methods may also be required and used where applicable. Emphasis is placed on accurate record keeping, along with photographic and detailed descriptions of any damage noted during the regular survey. These inspection methods are detailed in Sections 7 and 8 of Reference (4).

1.1.2 IFD-NDE Application History

Development of IFD-NDE for a specific structural application involves three phases. In the first phase, bar specimens of the structural material are evaluated utilizing the IFD technique and fatigue cycling the specimens. The second phase is a feasibility study where the technique is applied in the laboratory to a model or simulation of the physical system to be evaluated. The third phase involves application of the technique in the field. For the offshore structures program, the laboratory model phase is the initial phase as bar tests of structural steel were performed previously under other programs.

As a chronological example of the progression from laboratory to field application, the following three phase program regarding manned hyperbaric pressure chambers is discussed.

1.1.3 IFD-NDE Background

Initially, bar specimens 1" x 1" x 12" long were evaluated for the Naval Facilities Engineering Command (NAVFAC). These bar specimens were fatigued in flexure utilizing three point loading to a total of 10^5 cycles to fracture at room temperature. The materials were ductile steel (A514 and A537) with a yield stress of 100 ksi and 120 ksi. Six bars were notched and welded while the remaining six bars were notched and did not contain any welds. Base line data was evaluated for all bars before fatigue cycling began. Data was obtained at convenient intervals throughout the load cycle history of the bar specimens. Measured IFD values indicated incipient crack formation in all 12 bars, with cracking being predicted from 60 percent to 90 percent of the ultimate load cycle life of the various bar combinations (i.e., welded A514, unwelded A537, etc.). An important conclusion from the applied testing enabled the identification of a mismatch of weld material to base material to be made. This conclusion was supported by test data and subsequently confirmed by NAVFAC personnel.

The Naval Civil Engineering Laboratory (CEL) extended the application of the IFD-NDE technique to pressure vessels

of similar material as the bar specimens. Eight inch diameter by 37 inch long pressure vessels (.337 inch wall thickness) were constructed of Schedule 100-A53 steel. The vessels were notched along the longitudinal axis at the midspan so that failure would occur in approximately 10^4 load cycles. The pressure vessels were failed by applying pressure cycle loads of 3,000 psi; cycling the pressure between extremes of 50 psi and 3,000 psi. Base line data was collected and the fatigue cycling was initiated on the five pressure vessels. In all cases the IFD-NDE technique predicted incipient failure of the pressure vessels. The results of the tests indicated that the prediction of failure could be correlated to the measured specific damping capacity. Moreover, the prediction of incipient crack formation occurred at 80 percent to 90 percent of the ultimate life of the pressure vessels. The logical extension of the IFD-NDE technique from thin walled pressure vessels was further confirmed by the results of thick walled pressure vessel tests.

Two additional pressure vessels 60 inches in length and 18 inches in inside diameter with a three inch wall thickness were evaluated utilizing the IFD-NDE technique. These vessels were evaluated with the previously established test procedure which resulted in a failure prediction at 2,000 pressure cycles for Vessel 1 and 10,000 pressure cycles for Vessel 2. The vessels failed after 3,000 and 14,000 cycles respectively, although they were designed to rupture at approximately

100,000 cycles. Analysis of data from the pressure vessels also approximated the location of the crack that was correct within three inches of the actual crack (well within the limitation of the instrumented quadrant of the vessel). The failure was caused by a butt weld failure on an end plate. The pressure vessel did not crack along the machined notch as it was designed to do.

The results of the previously reported programs led to the application of the IFD-NDE technique to two large and complex hyperbaric pressure chambers. Results of tests conducted on laboratory pressure vessels provided base line data on the Ocean Simulation Facility (OSF) pressure chamber in Panama City, Florida and the Submarine Fluid Dynamics Simulation Facility (SFDSF) in Annapolis, Maryland. The OSF has three major systems which consist of a main chamber 15 feet in diameter and 40 feet long, a transfer chamber 12 feet in diameter and 15 feet long, and five smaller connected chambers measuring 6 feet in diameter and 6 feet long. Various on-site inspections including base line evaluation of the OSF pressure chamber have indicated no incipient crack formation has taken place. This result has been confirmed by frequent in-service inspection by the U. S. Navy Inspector General's proof load pressure cycle tests.

Additional IFD-NDE results were acquired on the SFDSF for both base line and in-service conditions. The results

of field tests indicated that an incipient crack was forming near a relief valve weld. Subsequent hydrostatic tests at 110 percent of yield opened the crack and demonstrated the successful application of the IFD-NDE technique in isolating and predicting the crack formation.

In addition to the pressure chamber tests, various component parts (cap bolts, bypass lines, primary piping systems, etc.) of nuclear reactors have been evaluated and are in the process of being field tested utilizing the IFD-NDE technique. The nuclear industry's inspection procedures are required to identify incipient failures because of the inherent safety requirements of the system. The field service test conditions in the reactor environment require internal pressure of 1100 psig, 550°F fluid temperature with flow conditions of 2500 gpm and mechanical loading of 1370 psig for the calculated hoop stress in the feedwater pipe system. Application of the IFD-NDE technique to drill string pipe, wire rope and synthetic rope specimens, confirmed the expected results of incipient cracking, material degradation and failure detection. The drill string pipe program initially correlated measured specific damping capacity to the use of the drill pipes. The internal friction damping values were recorded for numerous types of failed pipe, along with base line values of pipe which had not failed. Confidence limits were established and the resulting data base enabled a mathematical model to be postulated which

accounted for various individual and combined forms of degradation and failure. The established failure criteria based on the accumulated data was then correlated to the internal friction damping measurements. A specification based on the failure mechanism model and the rejection criteria that utilizes the IFD measurements is being established for drill string pipe. This specification will enable the user to define adequately that time in the load cycle history of the drill pipe that the pipe can no longer function as it was intended. The evaluation and confirmation of the failure mechanism model through field testing is being performed at this time.

1.2 Objective

The overall objective of this research program is to develop a nondestructive evaluation technique for the inspection of in-service offshore structures. This objective is to be fulfilled through the attainment of certain project milestones through a three phase program. Specific phase objectives are discussed in the next section.

1.2.1 Outline of Program Phase Objectives

As noted above, the completion of a research program concerning the application of an IFD-NDE technique to in-service offshore structures is projected to be accomplished in three phases. The three phases consist of two laboratory test phases and one field phase. The phases are outlined as follows:

PHASE I — Feasibility of applying IFD-NDE to 1/14 scale model offshore structure.

Feasibility of detecting structural degradation in model structure.

Feasibility of detecting missing members from transducers located above water line.

PHASE II — Laboratory evaluation of field instrumentation package and technique.

PHASE III — Field test and evaluation of prototype unit under actual in-service operating conditions, and field demonstration for cognizant personnel.

This technical report presents the engineering feasibility study and related results, obtained under the initial laboratory test phase. The data for the first phase was generated following the task statements outlined in the next section.

1.2.2 Task Statements - Phase I

Within this section the specific objectives under the current phase of the program will be discussed. These specific objectives are broken up into six task statements as follows:

TASK I — Modify the internal friction equipment and test techniques for generating engineering design data for application of IFD-NDE technique to complex structures.

TASK II — Design and construction of a model offshore structure for in-house laboratory testing.

TASK III — Measure the specific damping capacity (internal friction, $\frac{\Delta W}{W}$) of the model offshore structure fabricated in TASK II.

TASK IV — Fatigue members of the model structure to failure and obtain specific damping capacity measurements.

TASK V — Analyze the data generated under TASKS III and IV in order to optimize the engineering design parameters, reproducibility and reliability of the instrumentation required for the application to offshore structures.

TASK VI — Prepare a technical report and monthly progress reports that reflect the salient accomplishments of the program at specified intervals.

1.3 Scope of Program

In order to accomplish the overall objectives of the program leading to the development of a prototype IFD-NDE system for offshore structures, quantitative measurements of stress cycled members were made on a 1/14 scale model. The reliability and reproducibility for detecting failed members and joints was obtained by characterizing the change in internal friction damping for various members, caused by structural fatigue. Structural fatigue was accomplished by an electrohydraulic loading device, simulating waves, winds and other fatiguing conditions.

The 1/14 scale model of a Gulf Oil Corporation production platform (Figure 1) was constructed for the evaluation of the IFD-NDE technique. This design was used because it is a fixed permanent platform. By nature of its permanence, it is most susceptible to stress fatigue and dynamic loading.

2.0 THEORETICAL DEVELOPMENT OF INTERNAL FRICTION DAMPING

The theory presented in this chapter includes a discussion of internal friction damping on macroscopic and microscopic scales. The macroscopic view of internal friction damping is a relaxation process. The microscopic view considers the motion of dislocations which are pinned down by impurities and other dislocations. These two views are evaluated from the thermal diffusion coefficient and from the activation energy required to pass two dislocations over each other (11, 18).

2.1 Internal Friction Damping of Materials

It has been well known for over a century that materials manifest deviations from perfect elastic behavior even at small stress levels. Zener (5) called this behavior "anelasticity." Since real solids are never perfectly elastic, some of their mechanical energy is always converted into heat. The various mechanisms by which this occurs are collectively termed internal friction damping. Moreover, real solids exhibit a hysteresis loop whereby the stress-strain curve for decreasing stresses does not exactly retrace the upward path. Even though the offset in the magnitude of the hysteresis loop is negligible for static loading, it is an important factor in the dynamic response of a material. In addition to hysteresis, viscoelastic materials exhibit mechanical relaxation by an asymptotic increase in strain resulting from the sudden application

of a fixed stress; and conversely, by an asymptotic relaxation in stress whenever they are suddenly strained. This mechanical relaxation has an associated relaxation time, the direct result of which is the severe attenuation of vibrations whenever the imposed frequency has a period that approximates the relaxation time.

2.1.1 Specific Damping Capacity Definition

The most direct method for defining internal friction damping is by the specific damping capacity. Precisely, the specific damping capacity, Y, is defined by:

$$Y = \frac{\Delta W}{W} \qquad [1]$$

where:

ΔW = the energy dissipated in one cycle, and

W = the total energy of the cycle.

The mechanism by which the energy is dissipated may be any one of the following (6):

1. relaxation by thermal diffusion,
2. relaxation by atomic diffusion,
3. relaxation by magnetic diffusion,
4. relaxation by ordered distributions,
5. relaxation of preferential distributions,
6. stress relaxation along previously formed slip bands,

7. stress relaxation across grain boundaries, and
8. stress relaxation across twin interfaces.

2.1.2 Application of Internal Friction Damping

The phenomenon of internal friction damping of materials is used throughout the world to test authenticity of coins, the soundness of castings, the operating conditions of railroad wheels, and the quality of musical instruments and glassware by listening to the tone and duration of sound (7). The study of internal friction damping has been very useful as a research tool in physical metallurgy, in vibration control of high speed missiles, planes, and vehicles, in fatigue of materials, and in the study of the mechanical properties of viscoelastic materials from the standpoint of theoretical and analytical verification. There are various technical terms to characterize this phenomenon: internal friction damping, logarithmic decrement, hysteretic constant, viscosity, elastic phase constant, specific damping capacity, and so on. For the purposes of this report, internal friction damping describes the technique for utilizing the specific damping capacity of the 1/14 scale model offshore structure. Internal friction damping measurements are a standard technique (8-13) for evaluating how energy is absorbed as a function of changing material variables. These material variables include the grain size, the chemical composition, interstitial elements, dislocations, precipitate particles, strain rate effects, etc.

The evaluation presented in this report is the first research undertaken to apply the IFD-NDE technique to a complex structure.

2.2 Macroscopic Evaluation of Internal Friction Damping

From the theory of elasticity based on Hooke's Law, a body is considered in equilibrium under the action of applied forces when the elastic deformations take on static values. Many solids do not depart seriously from this perfectly elastic behavior for small deformations and the obtained results agree well with the predictions from the elastic theory. Within the realm of Hooke's Law, the only differences between individual solids results from differences in their elastic constants and their densities. However, when solids are subjected to forces that are rapidly changing, the response to these forces must be considered in terms of the dynamic elastic properties of the material (14).

2.2.1 Internal Friction Damping as a Relaxation Process

For viscoelastic materials, it was shown by Zener (15) that internal losses are the contributing factor for internal friction damping; and therefore, the mechanism of internal friction damping is described herein as a relaxation process. For vibrations whose frequencies are comparable with the time required for the relaxation process, there is an irreversible conversion of mechanical energy into heat which appears as internal friction damping. Zener (16) has solved this heat

transfer problem, and for vibrating strings the specific damping capacity is given by:

$$\frac{\Delta W}{W} = \frac{1}{2\pi} \cdot \left(\frac{TE\,\beta^2}{C}\right)\left(\frac{\omega\gamma}{\omega^2 + \gamma^2}\right) \qquad [2]$$

where:

$\gamma = (\pi/h)^2 D$,

ω = angular frequency

C = specific heat

β = thermal expansion coefficient

E = modulus of elasticity

T = temperature

D = thermal diffusion coefficient, and

h = specimen thickness

The maximum specific damping capacity occurs at frequency f_o which is obtained from equation [2] as:

$$f_o = \left(\frac{\pi}{2}\right)\left(\frac{D}{h^2}\right) \qquad [3]$$

The important physical interpretation of this work is that internal friction damping is a relaxation process. This process is governed by a characteristic time which corresponds to the "peak" frequency and is referred to as the relaxation time. Moreover, the internal friction damping resulting from the relaxation and diffusion process occurs whether or not the solid is homogenous. Within any viscoelastic material,

neighboring grains may have different crystallographic directions with respect to the direction of strain. Randall, Rose and Zener (17) have measured the internal friction damping in specimens of various grain sizes and found that, at the frequencies used, the maximum damping occurred when the size of the grain has an amplitude close to that predicted by equation [3].

2.2.2 Logarithmic Decrement

The specific damping capacity and associated dynamic response of the material is characterized by the damping coefficient or logarithmic decrement which can be expressed as:

$$\alpha = \left(\frac{1}{N}\right)\left(\ln \frac{A_o}{A_n}\right) \qquad [4]$$

where:

α = the damping coefficient,

A_o = the vibrational amplitude of the reference cycle, and

A_n = the vibrational amplitude after N cycles.

From the determination of α, the specific damping capacity $\left(\frac{\Delta W}{W}\right)$ for materials is calculated from the following equation:

$$\frac{\Delta W}{W} = 1 - e^{-2\alpha} \qquad [5]$$

2.3 Microscopic Evaluation of Internal Friction Damping

The macroscopic development of internal friction damping is a relaxation process. The microscopic evaluation determines the motion of dislocations that are pinned down by impurities and other dislocations. The microscopic evaluation is based on the mechanical behavior of grain boundary slip for crystalline materials.

2.3.1 Grain Boundary Interaction

Ke´ (18) used the ideas of internal friction damping as a relaxation and diffusion process in order to evaluate the mechanical behavior of grain boundaries for polycrystalline materials. By conducting experiments on the damping characteristics of pure materials, the corresponding internal friction damping produced by grain boundary slip was investigated. Moreover, Ke´ showed that internal friction damping could be related to grain boundaries behavior as a viscous material, and an elementary model for viscous slip along the grain boundary was constructed. The result of the model relates the coefficient of viscosity η of polycrystalline materials to their relaxation time τ as follows:

$$\eta = \left(\frac{d}{m}\right) E \cdot \tau \qquad [6]$$

where:

d = effective grain boundary thickness,

E = modulus of elasticity, and

m = grain size

Ke´ computed the coefficient of viscosity for pure aluminum by determining the elastic modulus from the natural frequency of vibration and by determining the relaxation time from internal friction damping measurements.

2.3.2 Disordered Groups

Another approach to the mechanism of viscous slip along the grain boundary was developed by Orowan (19), who considered disordered arrangements of atoms which are referred to as "disordered groups" or dislocations. By determining the stress distribution around the two critical atoms in the "disordered group", and by determining the shear process by which they can pass over one another, the following expression was obtained for the coefficient of viscosity of intercrystalline slip as:

$$\eta = \left(\frac{T}{s}\right) e^{H/RT} \qquad [7]$$

where the activation energy H is that which is required to pass the two critical atoms over each other, and s is the density of "disordered groups." By observing the viscous behavior of grain boundaries under small shearing stresses, King, Cahn, and Chalmers (20) showed that the mechanism of grain boundary slip in terms of "disordered groups" experimentally satisfied the mechanical behavior of the boundary.

2.3.3 Stress Relaxation Across Grain Boundary

Prior to Orowan's work, Ke´ (21) had considered the

relaxation dependence of internal friction damping, and of the modulus of elasticity for aluminum as a function of the frequency (f), and the grain size (m), of the specimen. It was demonstrated that the manifestations of internal friction damping can be expressed as a function of the parameter $(m \cdot f \cdot e^{H/RT})$, and a relationship was experimentally obtained for the specific damping capacity of aluminum as follows:

$$\frac{\Delta W}{W} \propto \left(m \cdot f \cdot e^{H/RT} \right) \qquad [8]$$

where H is the activation energy associated with the stress relaxation across the grain boundary arising from the viscous behavior of the grain boundaries.

2.3.4 Dislocation Density

A contributing factor to the internal friction damping results from the motion of dislocations which are "pinned down" by impurities, precipitates, and other dislocations. Internal friction damping for viscoelastic materials is sensitive to the amount of previous cold work and to the chemical composition of the material (22). By performing internal friction damping measurements made over several orders in magnitude range, Koehler (23) considered the effect of impurities on the logarithmic decrement. Viscoelastic specimens were subjected to external shearing stresses for a large range of frequencies and it was assumed that since diffusion is an extremely slow process at room temperature,

the impurity atoms are completely unable to follow the alternating stress. The dislocations were, therefore, anchored to the impurity atoms; and it was further assumed that the portion of the line dislocation between two impurity atoms oscillates on its slip plane like a stretched string. Thus, the fewer the impurities, the longer is the string length. Koehler solved the governing differential equation relating the applied shearing stress tending to move the dislocation along its slip plane to the equation of motion of the pinned down dislocation loop.

2.3.4.1 Dislocation Displacement

Koehler obtained expressions for the average displacement of a dislocation of a given length and for the shearing strain produced by this single loop in a cube of material of edge, L. Furthermore, from a consideration of a random distribution of atoms of solute along the dislocation line, an expression was obtained for the probability of finding two impurities separated by solvent atoms. The probability is directly proportional to the concentration of impurities, c, along the dislocation line. Finally, the logarithmic decrement was calculated by obtaining expressions for the energy loss per cycle and the total vibrational energy in the cycle. The specific damping capacity was found to vary with concentration of impurities as:

$$\frac{\Delta W}{W} \propto \frac{NBp^3}{c^4 L^3 E} \qquad [9]$$

where:

p = the interatomic spacing,

N = the number of atomic lengths of dislocation line, and

B = the damping force action on the dislocation.

Experimental verification of equation [9] is found in the fact that internal friction damping measurements conducted on copper after 40 hours exposure at 1,000°C in a vacuum showed that the logarithmic decrement was one order of magnitude greater than the logarithmic decrement of copper after 20 hours exposure at 1,000°C in hydrogen at atmospheric pressure. This dislocation concentration was further increased when a small percent by weight of iron was added to copper during melting and exposed to the above vacuum annealing. The logarithmic decrement for the copper-iron alloy decreased two orders of magnitude as compared to initial copper measurements.

2.3.4.2 Pinning of Dislocation Lines

Further verification of the theory regarding the change in internal friction damping by the pinning of free lengths of dislocation lines by impurity atoms is presented by Thompson and Holmes (24). Internal friction damping measurements were made on copper test specimens subjected to neutron bombardment. The investigators showed that the neutron damage adds to the effective impurity pinning already present through interstitial and vacancy atoms.

2.3.4.3 Relationship of Dislocation Density to Specific Damping Capacity

By eliminating the viscosity term from equations [6] and [7], the following expression is obtained:

$$\frac{d}{m} E\tau = \frac{T}{s} e^{H/RT} \qquad [10]$$

substituting the exponential term into the equation [8] gives:

$$\frac{\Delta W}{W} \propto f \, dE\tau \cdot \frac{s}{T} \qquad [11]$$

At the "peak" frequencies, $\tau = 1/f_o \simeq f$. Therefore, $\tau f \simeq 1$ for frequencies in the vicinity of the "peak" amplitude frequency. Equation [11] then becomes:

$$\frac{\Delta W}{W} \propto \frac{dE}{T} \cdot s \qquad [12]$$

This shows that the specific damping capacity is proportional to the dislocation density, s, which is the number of disordered pairs or the disordered density of the material. The disordered density of a material increases as the number of load repetitions increase. Figure 3 (25) illustrates the increase in the dislocation density as a function of the number of load cycles (ln N).

For cyclic loading of materials, slip bands (arrays of dislocations) will widen on the tensile cycle by slip interference, producing cross-slip dislocation. On the relaxation

cycle, dislocations at the edge of the bands are forced back through regions of relatively high defect density. Interactions between these dislocations and loops, point defects, and other dislocations effectively strain the existing structure so that nucleation of new slip lines is subsequently favored over widening of the old ones. Snowden and Grosskrentz (26) have investigated the dislocation structure by transmission electron microscopy. Figure 4 experimentally illustrates that the internal friction damping is closely correlated to the strain in the outer layers of the test specimen. This figure also shows the close dependent relationship between the internal friction damping and the strain in the outer layer. Moreover, it was observed that tangles formed on separated primary slip planes after only a few loading cycles. With continued cycling, these tangles spread into unstrained zones parallel to the slip planes. Transition from initial hardening to saturation coincided with the formation of a rather loosely knit, but regular cell structure. This structure remains relatively stable throughout the bulk of the useful fatigue life of the material. Dislocations and dislocation debris from this cell structure interacted at strain centers in the material. When the so-called "dormant" phase (27) was over (i.e., when dislocations were no longer able to move freely due to increasing debris and new slip and dislocation climb would initiate the crack formation process), the crack initiation slowly grew (Stage I) with each strain

increment; and then with increasing rapidity (Stage II), until the remaining cross-section fiber became small enough to break completely in a single tensile stroke. It is the defect distribution from the cell structure that is related to the specific damping capacity of the material. Moreover, corrosion fatigue stress accelerates failure because the corrosive media preferentially attacks the strain centers of the dislocation interactions and passivating films (28).

3.0 EXPERIMENTAL APPARATUS AND TECHNIQUE

This section details the experimental equipment necessary to generate the input response and monitor and analyze the output decay. Also discussed are the data reduction techniques.

Data analysis and associated equipment, both hardware and software that is required for the application of the IFD-NDE technique to the model structure will be discussed. Included is a discussion regarding the design and construction of the 1/14 scale model offshore structure, the electrohydraulic loading apparatus, and the associated loading harness. A schematic representation of the electronic equipment, the loading harness and the electrohydraulic loading device is shown in Figure 4.

3.1 Description of IFD-NDE Technique

The internal friction damping technique requires an input pulse with an associated output signal. The specific damping capacity $\left(\frac{\Delta W}{W}\right)$ is determined from the resultant decay curve of the output signal. Representative damping decay curves indicating changes in the internal friction for incipient crack detection are shown in Figure 5.

3.1.1 Input Signal - Source Vibration

In order to induce vibration in the structure, an electronic oscillator provides a continuous sinusoidal signal of specified frequency to a permanent magnet vibration exciter

(mini-shaker). Operation of a gating device interrupts the input signal and simultaneously triggers the storage oscilloscope which records the vibration decay.

3.1.2 Vibrational Response

Vibrational response of the model structure is measured by a piezoelectric accelerometer. The accelerometer converts the vibration to an electronic signal. Signal conditioning is accomplished by an audio frequency analyzer between the accelerometer and the storage oscilloscope.

The selection of the major components has to satisfy practical requirements to allow meaningful interpretation of results. Such design criteria require:

1. Frequency range: 20 - 20,000 Hz
2. High pick-up sensitivity
3. High signal/noise ratio
4. High accuracy of measurements
5. High amplification (100 dB)
6. Minimum harmonic distortion

A comparison of available equipment led to the selection of several commercially available instruments.

3.2 Description of IFD-NDE Instrumentation

A description of the electronic components is given in this section. The selected components are assembled as shown in Figure 6.

3.2.1 Frequency Oscillator

The Brüel and Kjaer sine generator Type 1023 is a precision signal generator covering the frequency range from 10 Hz to 20 kHz. The purpose of the frequency oscillator within the test apparatus is to generate a continuous periodic signal to drive the input transducer.

3.2.2 Vibration Exciter

The Brüel and Kjaer Type 4810 "mini-shaker" is of the electrodynamic type with a permanent field magnet. A coil is flexibly suspended in one plane in the field of the permanent magnet. An alternating current signal, provided by the oscillator, is passed through the coil to produce a vibratory motion. The mini-shaker is mechanically attached to the model structure as shown in Figure 7.

3.2.3 Accelerometers

Two different types of accelerometers were used to monitor the vibratory response of the model structure (Figure 9). They were a Brüel and Kjaer Type 4366 one-dimensional accelerometer and a Type 4321 three-dimensional accelerometer. The three-dimensional accelerometer consists of three individual accelerometer elements with their principal axes mounted such that it detects vibration in three mutually perpendicular directions. The main element of the accelerometers is a slice of piezoelectric quartz crystal which converts the vibrational response to an electronic signal by generating an electrical

charge across its pole faces which is proportional to the applied force.

3.2.4 Frequency Analyzer

The electronic signal from the accelerometers were input to a Brüel and Kjaer Type 2120 audio frequency analyzer. The frequency analyzer has been designed especially as a narrow band sound and vibration analyzer, and is of a constant percentage bandwidth. Incorporated into its design is an input amplifier, a weighting network, and a selective amplifier section (band pass filter). Its purpose within the test apparatus is to filter and amplify the output signal provided by the accelerometer.

3.2.5 Storage Oscilloscope

The storage oscilloscope is controlled by a voltage amplifier for the vertical axis and a time base for the horizontal axis. The voltage amplifier allows vertical amplitude adjustments of the signal. The time base controls the sweep rate of the electron beam in the horizontal direction. The oscilloscope is externally triggered by the gating device so that the trace begins simultaneously with the interruption of the input signal to the mini-shaker. The trace continues as the vibration of the model structure decays, recording the output amplitude as a function of time. A photograph is taken of the stored trace and later analyzed to yield the specific damping capacity values $(\frac{\Delta W}{W})$. Tektronix Model 7613 was used as the storage oscilloscope in this program.

3.2.6 Spectrum Analyzer

The digital frequency analyzer, Brüel and Kjaer Type 2131 is designed to measure and display octave and one-third octave spectra in real-time. The frequency spectrum analysis made possible the identification of the major resonant peak frequencies of each member and joint whereby the characteristics of each individual output could be analyzed.

3.2.7 Digital Computer

The digital computer and associated software provides the capability for reduction of the data acquired with the previously described IFD-NDE instrumentation. Data reduction was accomplished in this initial program phase in the following manner.

Employing the IFD-NDE instrumentation, an output signal decay curve is generated and stored on the oscilloscope CRT. A photograph of this decay envelope is made and manual reduction of the photograph takes place. This information is then input to the computer and processed by the in-house software program. Specific damping capacity values $\left(\frac{\Delta W}{W}\right)$, standard deviations and statistical analysis data are obtained as an output. The system for this task was a Digital Equipment Corporation (DEC) PDP 11/34.

3.2.8 Instrumentation Calibration

The calibration of the test apparatus is performed in two steps. The driving signal is calibrated during the first

step and the output decay signal is calibrated as a second step.

To calibrate the driving signal, a continuous vibration of the specimen over the frequency range of the frequency oscillator is made. This procedure enables the determination of the natural frequencies of the specimen, since each specimen may have different frequencies.

The calibration of the output vibration decay for accurate recordings consists of two parts. First, the output signal amplitude is optimized using different levels of amplification such that the steady state vibration signal amplitude occupies the full vertical scale on the oscilloscope CRT. Then the time spread of the vibration decay is set to occupy between 5 to 10 centimeters on the oscilloscope display.

At this point, the calibration of the experimental test apparatus is completed and a permanent recording of the output signal can be performed. This permanent recording can be achieved either on the oscilloscope (storage memory) or on the level recorder (tracing of the decay slope on calibrated strip-chart paper).

3.3 Design and Construction of 1/14 Scale Model Offshore Structure

A literature search was conducted which included an investigation of the designs, uses, and classifications of offshore

structures. The search dealt with an analysis of typical failures as well as the complexities encountered in structural integrity inspections.

As a result of this search, the structure type chosen for this NDE program was the fixed, permanent platform. By nature of its permanence, this structure is most susceptible to stress fatigue and corrosion fatigue. The permanent platform is also most susceptible to dynamic loading as a result of its fixed bottom. It was found that the fixed platform is the most economical of the four major platform types in shallow depths.

The next step undertaken was to choose a typical structural design to be modeled. It was found that fixed platforms are generally used in depths characteristic of most of the continental shelf. The final in-house design is identical in member configuration to the Block 48, Platform B, Gulf Oil Corporation production platform at South Marsh Island.

The in-house model was fabricated with actual structural materials, construction, and assembly parameters in a similar fashion as an offshore tower. The model tower structure, derived from the overall literature search, was designed and constructed to 1/14 scale. The approximate height of the tower is 14 feet with the main columns 1-1/2 inches in diameter. The support bracing is 3/4 inches in diameter to maintain consistent scaling parameters. All material in the structure is steel pipe. The vertical columns and redundant bracing divided the

tower into four symmetrical faces. The redundant nature of the tower parallels actual offshore structures which are redundantly braced to maintain associated factors of safety.

All bracing members were welded to maintain structural integrity. The individual welded sections that comprise the bracing system for the four main columns of the scale model offshore platform were contoured on each end before being welded into the structure. The curvature of the members matches the surface of the mating piece so that the contact between the two joined pieces was maximized. This procedure follows acceptable American Institute of Steel Construction (AISC) welding standards and simulated field construction of full size offshore towers.

3.4 Design and Construction of the Electrohydraulic Loading Device

An electrohydraulic loading device was designed and constructed to function with a hydraulic cylinder as the fatigue loading machine. The directional control of the cylinder stroke was governed by a General Radio tone burst generator, whose signal actuated a solenoid operated directional valve.

Additionally, a hydraulic pump and peripheral equipment was designed and assembled into a unit capable of driving the loading cylinder. The system is capable of two gallons per minute flow rate and a maximum pressure of 3,000 psig. The operating pressure is controlled by a Sperry Vickers relief valve. Figure 9 is a graphical representation of the electrohydraulic loading apparatus.

3.5 Design and Construction of Specimen Loading Fixture

The hydraulic cylinder was rigidly connected to a loading harness, in turn supported by two of the main columns. Load was transmitted from the cylinder rod to the member being failed through a rotational swing arm. The swing arm was pin-connected to the loading harness at one end and attached to the specimen member at the other end. The stiffness of the loading harness was approximately twenty times the stiffness of the member being failed.

3.6 Data Analysis

3.6.1 Introduction to Data Analysis

The output decay of the IFD-NDE technique is a logarithmic decay of the system response resulting from the input pulse. From the record of the output decay, a reference amplitude (A_o) is measured. $A_{n(1-5)}$ is defined at five equal cycle intervals of the decay interval. The ratio of the relative amplitudes (A_o/A_n) is determined for the five amplitudes. The logarithmic decrement is determined from equation [4] which provides $\alpha_{n(1-5)}$. The specific damping capacity is determined from equation [5] and provides $\frac{\Delta W}{W}_{n(1-5)}$.

Utilizing measured values of specific damping capacity over the work-cycle history of the material in a linear least-squares fit, an equation for the base line value specific damping capacity can be generated in the form:

$$\left[\frac{\Delta W}{W}\right]_{est} = a(LC_n) + b \qquad [13]$$

where:

$\left[\frac{\Delta W}{W}\right]_{est}$ = estimated specific damping capacity, and

LC_n = number of load cycles

and a and b are constants determined from the data. Additionally, from the data, a standard error of estimate can be determined for $\frac{\Delta W}{W}$ on LC_n from:

$$S\left(\frac{\Delta W}{W} \cdot LC_n\right) = \left[\frac{\sum\left(\frac{\Delta W}{W} - \left[\frac{\Delta W}{W}\right]_{est}\right)^2}{LC_n}\right]^{\frac{1}{2}} \quad [14]$$

where:

$S\left(\frac{\Delta W}{W} \cdot LC_n\right)$ = standard error of estimate

$\frac{\Delta W}{W}$ = measured specific damping capacity

$\left[\frac{\Delta W}{W}\right]_{est}$ = specific damping capacity from equation [13]

a bandwidth of $3S\left(\frac{\Delta W}{W} \cdot LC_n\right)$ can be established for equations wherein 99.7% of the data used to determine the equation are included within the band. At the point of failure initiation, the increase in the measured value of specific damping capacity will be found outside the bandwidth for the established base line equation.

Equation [14] represents the base line value of specific damping capacity for the bar test samples prior to the initiation of material failure. The standard error of estimated bandwidth is defined by:

$$\left(\frac{\Delta W}{W}\right)_{est} \pm 3S\left(\frac{\Delta W}{W} \cdot LC_n\right) \qquad [15]$$

3.6.2 Data Reduction Program

The program associated with the calculation of the specific damping capacity is found in Appendix A. The initial procedure sets the memory bank to zero and the reference amplitude (A_o) is entered into the program. The number of decay cycles (N) between subsequent relative amplitude measurements (A_n) is entered into the program. The logarithmic decrement is calculated and the least-squares linear curve fit is performed on the data. The specific damping capacity is determined along with the standard deviation of the least-squares linear fit. The data reduction program is found in Appendix A along with the definition of the sample mean, sample variance, and least squares curve fit.

4.0 EXPERIMENTAL TEST PROCEDURES, RESULTS AND DISCUSSION

This section presents the test matrix, various test techniques, data acquisition, and a discussion of the results from the application of the IFD-NDE technique to the 1/14 scale model offshore structure.

4.1 Preparation of Model Offshore Structure for Testing

4.1.1 Model Offshore Structure Instrumentation

Prior to data acquisition, the model offshore structure was instrumented with the mini-shaker and the accelerometers. The mini-shaker was mechanically attached to a top central location on the model structure.

For this laboratory investigation, only one side (face) of the model structure was monitored at a time. An accelerometer was mounted on one of the two redundant members of each of the four bays, which make up the structure face. The accelerometers were located at the midspan of each instrumented member. These sites for mounting were chosen because, in the two transverse modes of vibration (X, Z), maximum displacement would be expected to occur at that point. (This results from the analysis of the end points being fixed.) The third mode, longitudinal to the member (Y), is not adversely affected by placement, as one would expect relatively constant pulse amplitude in that mode. Figure 10 depicts schematically the accelerometer locations and orientations.

4.1.2 IFD-NDE Analysis Test Matrix

The test matrix is divided into two tables, the preliminary frequency response tests (Table 1) and the fatigue cycling tests (Table 2). The preliminary frequency response tests were comprised of four tests; one-dimensional frequency analysis, attachable collar, thermal stress and hole drilling (member damage).

Table 2 presents the preliminary tests. The one-dimensional frequency analysis was performed to determine frequency relationships between the instrumented members. The next test consisted of attaching a collar to various members of the instrumented side of the tower. In the thermal stress test, heat was applied to the instrumented member in the third bay. Holes were also cut into the instrumented member in bay number three to observe the effect of damaging the member.

Table 2 is comprised of three fatigue tests. In the first test, one-dimensional accelerometers were mounted at midspan on one redundant member in each of the upper three bays. The fourth output accelerometer was mounted on the member being fatigued. The test notch was located at midspan of the member being fatigued. Cycling started at 30 percent of yield for approximately 37,000 cycles and then increased to 45 percent of yield until a crack appeared.

The second test had one-dimensional accelerometers mounted at midspan on one redundant member in each of the upper two

bays. Three-dimensional accelerometers were mounted at midspan on one redundant member in bay three and on the member being fatigued. Test Notch I was located at midspan of the fatigued member. Cycling was done at 75 percent of yield until a crack appeared, at which time cycling stopped.

In the third test three-dimensional accelerometers were mounted on one redundant member in each of the four bays of the model structure. Test notches were located, in order of failure: at Weld II, between the vertical leg and fatigued member; Weld II, instrumented redundant member in bay 3 and fatigued member; Weld IV, vertical leg and fatigued member; and Weld V, redundant member in bay 3 and fatigued member. For each weld failure a calculated load of 75 percent of yield was induced. Figure 11 shows the weld/notch locations on the model offshore structure.

4.2 One-Dimensional Analysis of Model Structure Response

4.2.1 Frequency Response

An initial sweep of the frequency spectrum was made for each member instrumented in order to find their resonant frequencies. Resonant frequencies are defined as frequencies of peak vibratory response. Using the spectrum analyzer allowed peak frequencies from the overall audio frequency spectrum (20 Hz to 20,000 Hz) to be displayed (Figure 12). Once the peak frequencies were identified, the oscillator was adjusted to each one in turn. When a resonant frequency was identified

for a given member, the output amplitude was recorded and then compared to the output amplitude of the other instrumented members. In doing this, it was found that each of the instrumented members had a few primary resonant frequencies with a relatively high output amplitude and several secondary resonant frequencies of lower amplitude. It was also noted that the model structure has an overall structural resonance of approximately 630 Hz.

4.2.2 Attachable Collar Test

The attachable collar test was designed to see what effect, if any, a large mass would have on the vibrational response of a given member. The collar was machined so that it could be easily attached to any bracing member of the model structure. It was of enough mass (approximate weight 7.5 pounds) to cause damping of the vibrational response of that member.

A frequency scan was made and frequencies that produced outputs of relatively high magnitudes were chosen and recorded for the four accelerometer locations. The collar was then attached to the various members on the instrumented side of the model structure. The frequencies were then retuned and outputs recorded. The result was that by employing relative frequency shifts and changes of magnitude of the output response it could be determined to which member the collar was attached.

4.2.3 Thermal Stress Test

Thermal stress was induced into the model structure using an acetylene torch. The heating of different members showed drastic changes in output amplitude and relatively small frequency shifts while hot. As the member cooled, the outputs and frequencies returned to the original base line. It could be determined from the changes in frequencies and output amplitudes which member was being heated.

4.2.4 Hole Drilling Tests

Holes were machined in members to determine what effect this would have on the measured values obtained for the tower. The established frequencies were monitored before, during, and after the holes were made. Data analysis showed no significant changes in output amplitude or specific damping capacity values.

This is in line with theoretical expectations, as sawing a hole does not change the material properties of the components.

4.3 Changes in Specific Damping Capacity Resulting from Fatigue Cycling Tests Using One-Dimensional Analysis

Specific damping capacity measurements were obtained by applying the IFD-NDE instrumentation and technique to the 1/14 scale model offshore structure at various times in the fatigue cycle history. Prior to fatigue cycling, the loading harness was mounted on the model structure. A preliminary sweep of the frequency spectrum showed minor shifts of the resonant frequencies caused by additional mass of the load harness.

The member being fatigued was notched on the tensile side at midspan. When the member was subjected to cyclic bending, a stress concentration at the notch would allow crack initiation to occur at that location. The notch size was .04 inches deep, .06 inches wide, and .44 inches long.

The initial base line data points were then taken, one resonant frequency was chosen for each accelerometer location. At this point fatigue cycling began. A calculated load (Appendix B) of 270 pounds was then applied. This caused extreme fiber stress of 30 percent of yield stress at midspan.

One cycle consisted of 0.5 second load application followed by 0.25 second relaxation. After 37,000 cycles, microscopic examination, using a 10 power filar microscope eyepiece, revealed no cracks in the member. The load was then increased to 405 pounds inducing extreme fiber stress of 45 percent of yield at midspan. Cycling continued until load cycle 97,367 when a microscopic crack was observed in the root of the notch.

The data obtained in this first test yielded no indication as to the condition of the model structure, and therefore, prediction of a failure could not be made. However, sufficient indications as to the guidelines for the following tests were obtained. This test showed that after fatigue cycling began, some frequencies which initially showed reproducible decay shapes, quickly deteriorated and could no longer be used. Moreover, the susceptibility to floor vibrations was noted

and data acquisition procedures were redesigned accordingly. The scatter in data from this one-dimensional analysis indicated that the output specific damping capacities of the structural members that would predict cracking were probably contained in other modes of vibration. This hypothesis led to the application of the three-dimensional accelerometers in tests two and three.

4.4 Changes in Specific Damping Capacity Using Three-Dimensional Analysis of Midpoint Crack Detection

During this fatigue cycling test the model structure was instrumented with one-dimensional accelerometers on one redundant member in each of the upper two bays. This permitted the vibrations normal to the face plane of the model structure to be monitored. The three-dimensional accelerometers were mounted on one redundant member in bay 2, and the member being fatigued, approximately four inches from the test notch (Figure 10). The three-dimensional accelerometers allowed three mutually perpendicular axes of vibration of the member to be monitored. The member being fatigued was again notched at midspan (.047 inches deep, .086 inches wide, .57 inches long) allowing crack initiation to occur at that location.

After the initial frequency sweep two to three frequencies where chosen for each vibrational mode at each accelerometer location. A total of twenty resonant frequencies were

observed. Table 3 shows the resonant frequencies chosen for each accelerometer location and vibrational mode. Base line specific damping capacity measurements were then recorded and fatigue cycling began.

A load of 675 pounds was applied inducing an extreme fiber stress of 75 percent of yield at midspan. Cycling continued until 9,000 cycles when a microscopic crack was observed in the root of the test notch. Crack growth was slow but steady until cycle 11,500 when growth accelerated. Cycling was stopped at cycle 13,500 when the member was cracked three-quarters of the way through. Specific damping capacity measurements were taken throughout fatigue cycling.

The results obtained from this test yielded indications that crack initiation and growth were monitored by the IFD-NDE technique. Three illustrations of data follow the trends in data which are anticipated; that is, base line points, rising $\frac{\Delta W}{W}$ values indicating stress concentrations forming, followed by descending $\frac{\Delta W}{W}$ values showing the release of crack site energy as the crack increases. Figures 13a and 13b show the results as plotted for Member C at 3,312 Hz for both the X and Y orientations. The peak in these curves would seem to indicate that crack formation began in the region of 8,000 cycles with actual crack initiation around 8,500 cycles. The

downturn of the curve relates to the loss of crack site energy as the crack enlarged. Member C a 751 Hz (Figure 13c) indicates that crack initiation occurred in the region of 7,000 cycles. A release of crack site energy seems to have occurred in the region of 8,500 cycles. Data obtained from the other instrumented members yielded no supportive results.

4.5 Three-dimensional Analysis of Member Failure

At this time cognizant personnel expressed a desire to see data beyond the crack initiation state to member failure. It was also pointed out that most failures of offshore structures occur at weld locations. As a result, test procedures were modified to include complete failure of welds along a horizontal member of the model structure. Test notches were machined at the four weld locations along the horizontal member being fatigued (Figure 11).

During this test one diagonal member in each of the four bays on the same face as the member to be failed, was instrumented with three-dimensional accelerometers. Figure 10 shows accelerometer locations and vibrational modes monitored for each member. Base line data was then taken at the four accelerometer locations; two resonant frequencies were chosen for each of the three axes of vibration. Table 3 shows the frequencies observed for each member and vibrational axis. A load of 75 percent of yield at the welds was applied and cycling began.

the member was failed at each weld location and the member was broken free from the model structure.

Specific damping capacity measurements ($\frac{\Delta W}{W}$) recorded during this test indicate trends which are indicative of crack formation and growth. These trends were noted at all four accelerometer locations. As the member progressed through the various failure stages, the logarithmic decay envelope became increasingly degraded, varying from a highly damped exponential to that of an irregularly shaped decay envelope (Figure 14). Data reduction was not carried out past the initial break at Weld II (see Figure 11) because the decay envelope was so degraded that it could not be reduced with the high level of confidence normally utilized.

The measured specific damping versus fatigue cycle graphs shown in Figures 15 and 16 show the trends which are expected from past experience. Figure 15 includes five graphs which indicate IFD detection of a crack at Weld I using a 99 percent upper confidence limit. The largest increase in $\frac{\Delta W}{W}$ at the time of cracking was noted at accelerometer Location C, in the longitudinal mode of vibration at 813 Hz (Figure 15-a). Accelerometer Location C is at midspan of the diagonal directly above the member subject to failure. This diagonal member is connected to the failed member at midspan, and therefore, would be expected to be most affected by the crack. Specific damping capacity values were also significantly outside the

upper confidence limit at the time of cracking for the transverse vibrational mode of 2740 Hz, normal to the tower face plane at Location C; and the longitudinal 1086 Hz and transverse in plane 2050 Hz modes at Location D. Accelerometer Location D was midspan of the diagonal directly below the failed member. The transverse, in plane 1870 Hz mode for accelerometer Location B also indicated the crack ($\frac{\Delta W}{W}$ exceeded the 99 percent confidence limit). The increase in $\frac{\Delta W}{W}$ for this location was not as great as the others just mentioned, however, this is expected as Location B was in the second bay above the failed member.

Figure 16 includes seven graphs which indicate IFD detection of the broken joint at Weld II. Specific damping capacity values for the higher frequency longitudinal resonances at accelerometer locations B, C, and D all indicated the change in the structure when the weld broke (Figures 16 a, b, c, f). Measurement of the damping of the transverse mode normal to the face plane at 2360 Hz for Location C also showed an increase when the member failed (Figure 16d); as did the transverse, in plane, 4210 Hz mode at Location D (Figure 16e). It is especially noteworthy that the break in Weld II was detected as far away as accelerometer Location A, in the top bay of the model structure (Figure 16g). This lends support to the hypothesis that detection of broken joints in actual offshore structures, using IFD-NDE, may be possible through instrumentation of the upper, most accessible areas.

5.0 CONCLUSIONS

This section presents conclusions based upon data and results reported in Section 4.0 of this report.

5.1 Applying IFD-NDE Instrumentation to the 1/14 Scale Model Offshore Structure

This report demonstrates that the IFD-NDE instrumentation is applicable to the 1/14 scale model structure. Existing laboratory equipment was modified, as described in Section 3.0, for this application of the IFD technique.

5.2 Obtaining Frequency Response Data from Individual Members of a Complex Structure

This report concludes that individual members can be excited to a resonant frequency and the IFD instrumentation is able to monitor these frequencies. This conclusion is based upon the one-dimensional analysis of the model structure frequency response (Section 4.2.1) where individual frequencies were identified and outputs recorded.

5.3 Monitoring Changes in Base Line Frequency Response of the Model Structure's Members

This report concludes that the IFD instrumentation can monitor changes in the integrity of the model structure. This conclusion is based upon the changes in output on the minor frequency shifts which occurred during the attachable collar test and the thermal stress test.

5.4 Generating Internal Friction Damping Data from the Model Structure's Members

This report demonstrates the ability to obtain specific damping capacity measurements from the model structure. This is based upon the initial laboratory testing, where the model structure, in an unstressed state, was excited by an input signal and then gated. This allowed the model structure to dampen naturally at that driven frequency. The resulting logarithmic decay envelope was then reduced to a specific damping capacity value.

5.5 Utilizing Internal Friction Damping Data to Monitor the Model Structure's Member While Undergoing Fatigue Cycling and Failure

This report concludes that the IFD-NDE technique is capable of monitoring the model structure's various stages of degradation. This conclusion is based upon the specific damping values recorded during fatigue cycling. It was also noted that the frequencies that monitored the structure's degradation are in predominantly two axes of vibration. From a point that would correspond to above water line on an actual offshore structure, the degradation of the structure could be observed.

5.6 Primary Test Frequency Signal to Noise (S/N) Ratio

During fatigue cycling, it was discovered that the established base line frequencies had only minor frequency shifts;

less than one percent. Even though the logarithmic decay envelope became increasingly degraded such that they could not be reduced for specific damping capacity values, none of the output levels for the base line frequencies dropped below the noise threshold.

6.0 RECOMMENDATIONS FOR FURTHER WORK

Successful completion of this feasibility phase of the program as evidenced by the engineering data provided the incentive to recommend further work. The following suggestions are made as a continuation of this feasibility program.

6.1 Initiating Field Trips with Laboratory IFD-NDE Equipment to Determine Engineering Problems Encountered in Instrumenting an In-Service Offshore Structure

During these trips a determination will be made as to whether the equipment as used in the laboratory will suffice as the operational unit. The salient results from the experimental program will be evaluated which will enable the contractor to perform a final prototype design of the nondestructive evaluation unit that will serve as the operational on-line equipment. This design procedure will utilize inputs that are typical of field use such as the need for equipment that can withstand changing environmental conditions or perform in a dynamic state.

6.2 Assembling of Detailed Test Plan that will Enable Acquisition of Data from Various Types of In-Service Offshore Structures

The test plan will enable the contractor to identify the system characteristics that cause failure in the various types of offshore structures. The planning document will include the necessary contact with cognizant personnel to design the

experimental analysis and to establish the input/output design parameters that will be used in the final equipment package.

6.3 Certifying the Prototype IFD-NDE Instrumentation Package as Intrinsically Safe for Use on In-Service Offshore Structures

The equipment identified under the program for the purpose of detecting incipient failure in offshore structures will be certified as intrinsically safe. The equipment manufacturers shall be requested to provide substantive data consisting of electronic schematics, code approved designs, and field test results for the purpose of evaluating the intrinsically safe nature of the package. The equipment selected will meet all necessary requirements for use on offshore structures. Moreover, the instrumentation package will be guaranteed as intrinsically safe for operations on offshore structures.

6.4 Generating Specific Damping Capacity Measurements (Internal Friction) from Various Types of Offshore Structures

Using laboratory equipment, specific damping capacity measurements will be taken from various types of offshore structures. These measurements will be tested for reliability and reproducibility (at a 99 percent confidence level) for a given single measurement compared within similar sets of data.

6.5 Collecting and Evaluating Data Generated Under Section 6.4 in Order to Evaluate the Method for Detecting Incipient Failure Modes

The data collected from the various offshore structures will be analyzed as was done in Section 3.7 of this report. The data will then be correlated to the various offshore structures in order to establish a fatigue life history.

6.6 Design and Assembly of Prototype Field IFD-NDE Instrumentation Package for Automatic Data Acquisition

The present software will be utilized to determine the $\frac{\Delta W}{W}$ value for specific components and combine that software with other software developed to classify flaw and failure mechanisms. The frequency spectrum analysis program which is derived from the fast fourier transform performed on the waveform output from the frequency analyzer could be utilized along with the digital processor to accomplish this task. The objective of this task would be to combine the existing technology with the existing software and apply the analysis technique to representative members of offshore structures. With the extension of the software as identified in this technical proposal, the complete internal friction damping (IFD) technique could be performed automatically. The output from this task would be the automatic acquisition, storage, analysis, retrieval, and comparison of $\frac{\Delta W}{W}$ values that would lead to predicting the ultimate failure of components.

6.7 Selection of Field Site to Demonstrate the Prototype Test Equipment and Technique to Cognizant Government Personnel

The field demonstration would occur under actual on-site operating conditions and would be conducted during a one month test period. The purpose is to indicate to the cognizant government personnel the application of the NDE internal friction technique. Under this task, the technology would be transferred to the operators and end-users (inspection teams).

REFERENCES

1. Quinn, Alonzo, Def. Design and Construction of Ports and Marine Structures. New York: McGraw Hill Book Corporation, 1961.

2. Fresch, D. C., L. L. Yeager, A. A. Hochrein, Jr., and A. P. Thiruvengadam. "Preliminary Testing Results for the Application of a Nondestructive Evaluation Technique Utilizing the Phenomenon of Internal Friction for Detecting Crack Formation in a Scale Model of an Offshore Structure." DAI Technical Report DF-7763-001-TR. September, 1978.

3. American Society of Metals. Metals Handbook.

4. American Petroleum Institute. API Recommended Practice for Planning, Design and Construction of Fixed Offshore Platforms. Texas: 300 Corrigan Tower Building, Dallas, 75201, April 1977.

5. Zener, C. "Internal Friction in Solids, Theory of Internal Friction in Reeds." Physical Review, Volume 52, 1937, page 230.

6. Zener, C. "Elasticity and Anelasticity of Metals." Chicago: The University of Chicago Press, 1948.

7. Jenson, J. W. "Damping Capacity - Its Measurement and Significance." Bureau of Mines Report of Investigation, 5441. United States Department of the Interior, 1959.

8. Grosskrentz, J. C. Fatigue an Interdisciplinary Approach. New York: Syracuse University Press, 1964, page 27.

9. Roberts J. T. A., and P. Barrand. "Model for the Low Temperature Grain Boundary Damping Peak in FCC Metals." TRANS. AIME 242, 1968, pages 2299-2303.

10. Roberts, J. T. A. "Grain Boundary Damping in Substitutional Alloys." MET. TRANS. 1, 1979, pages 2487-2493.

11. Peguin, P., J. Perez, and P. Gobin. "Amplitude - Dependent Part of the Internal Friction of Aluminum." TRANS. AIME 239, 1967, pages 438-451.

12. Sachse, W., and R. E. Green, Jr. "Experimental Study of the Orientation Dependence of Dislocation Damping in Aluminum Crystals." TRANS. AIME 242, 1968, pages 2185-2190.

13. Gilba, R. "Internal Friction in Hydrogen Charged Iron." TRANS. AIME 239, 1967, pages 1574-1584.

14. Kalski, H. "Stress Waves in Solids." New York: Dover Publications, 1963.

15. Zener, C. "Internal Friction in Solids, Theory of Internal Friction in Reeds." Physical Review, Volume 52, 1937, page 230.

16. Zener, C. "Internal Friction in Solids, General Theory of Thermoelastic Internal Friction." Physical Review, Volume 53, 1938, page 90.

17. Randall, R. H., F. C. Rose, and C. Zener. "Intercrystalline Thermal Currents as a Source of Internal Friction." Physical Review, Volume 56, 1939, page 343.

18. Ke, T. S. "Experimental Evidence of the Viscous Behavior of Grain Boundaries in Metals." Physical Review, Volume 71, 1947, page 533.

19. Orowan, I. E. "Mechanism of Viscous Flow in Solids." Proceedings West of Scotland Iron and Steel Institute. 1947.

20. King, R. R., W. Cahn, and B. Chalmer. "Mechanical Behavior of Crystal Boundaries in Metals." Nature, Volume 161, 1948, page 682.

21. Ke, T. S. "Stress Relaxation Across Grain Boundaries in Metals." Physical Review, Volume 72, 1947, page 41.

22. Seitz, F. Physics of Metals, Chapter Ten. New York: McGraw-Hill Book Company, 1943.

23. Koehler, J. S. "The Influence of Dislocations and Impurities on the Damping and the Elastic Constants of Metal Crystals." Imperfections in Nearly Perfect Crystals, Edited by W. Shockley. New York: John Wiley and Sons, Inc., 1962, page 191.

24. Thompson, D. O., and D. K. Holmes. "Dependence of Young's Modulus and Internal Friction of Copper Upon Neutron Bombardment." Journal of Applied Physics, Volume 27, 1956, page 191.

25. Carson, K. R., and J. Weertman. "Dislocation Density in Single Crystals of Silicon-Iron During Low Cycle Fatigue." TRANS. AIME 242, 1968, pages 956-958.

26. Boettner, R. C. "Fatigue Crack Nucleation in a High Strength, Low-Alloy Steel." TRANS. AIME 239, 1967, pages 1030-1033.

27. Cotrell, A. H. The Mechanical Properties of Matter. New York: John Wiley and Sons, Inc., 1964.

28. Thiruvengadam, A. P. "On Corrosion Fatigue at High Frequencies." American Society for Testing and Materials. STP 503, 1970, page 171.

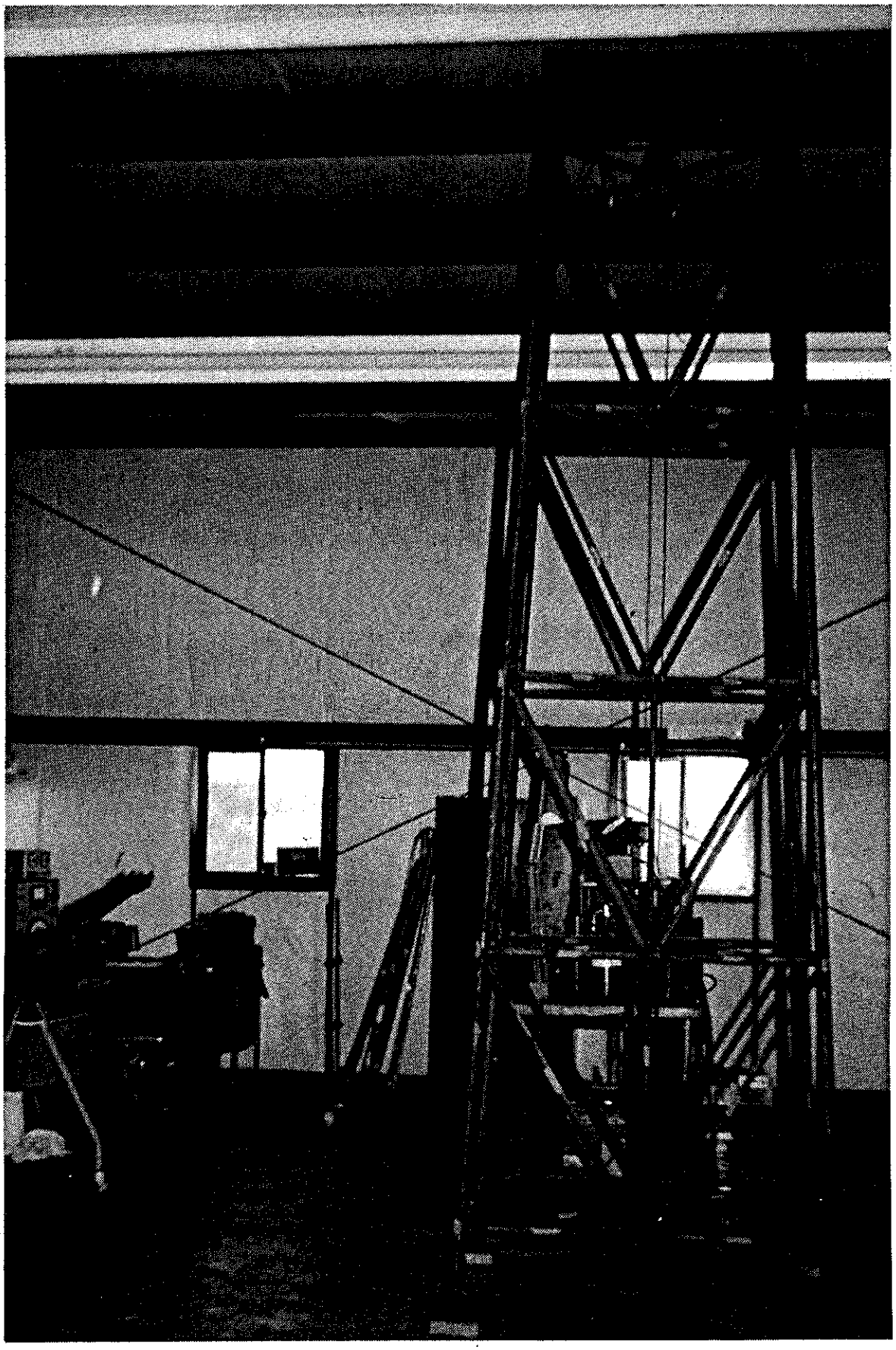

FIGURE 1 1/14 SCALE MODEL OFFSHORE STRUCTURE USED IN INTERNAL FRICTION DAMPING NONDESTRUCTIVE TESTING

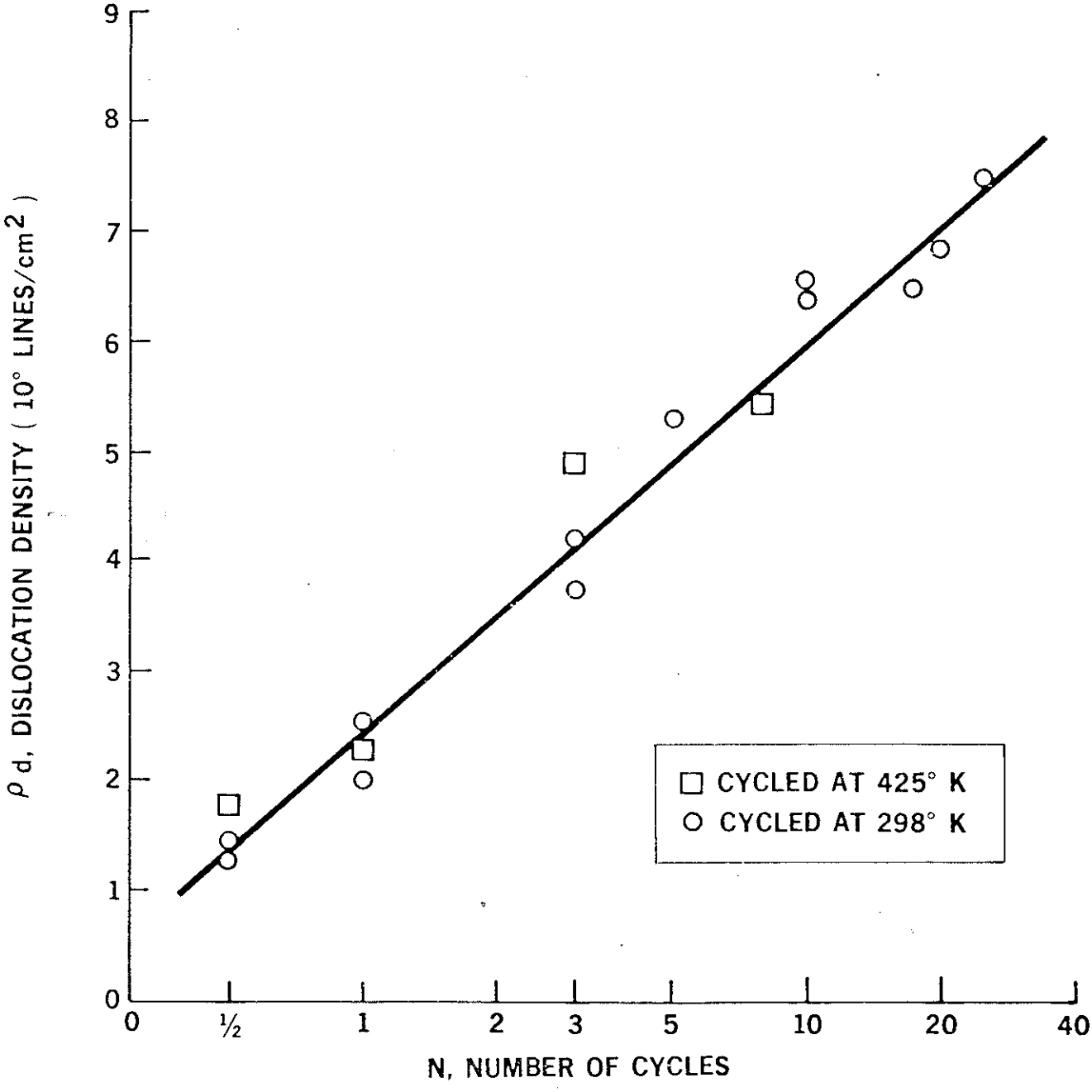

FIGURE 2 THE OVERALL DISLOCATION DENSITY, ρd, AS A FUNCTION OF THE NATURAL LOG OF THE NUMBER OF CYCLES, $\ell_n N$

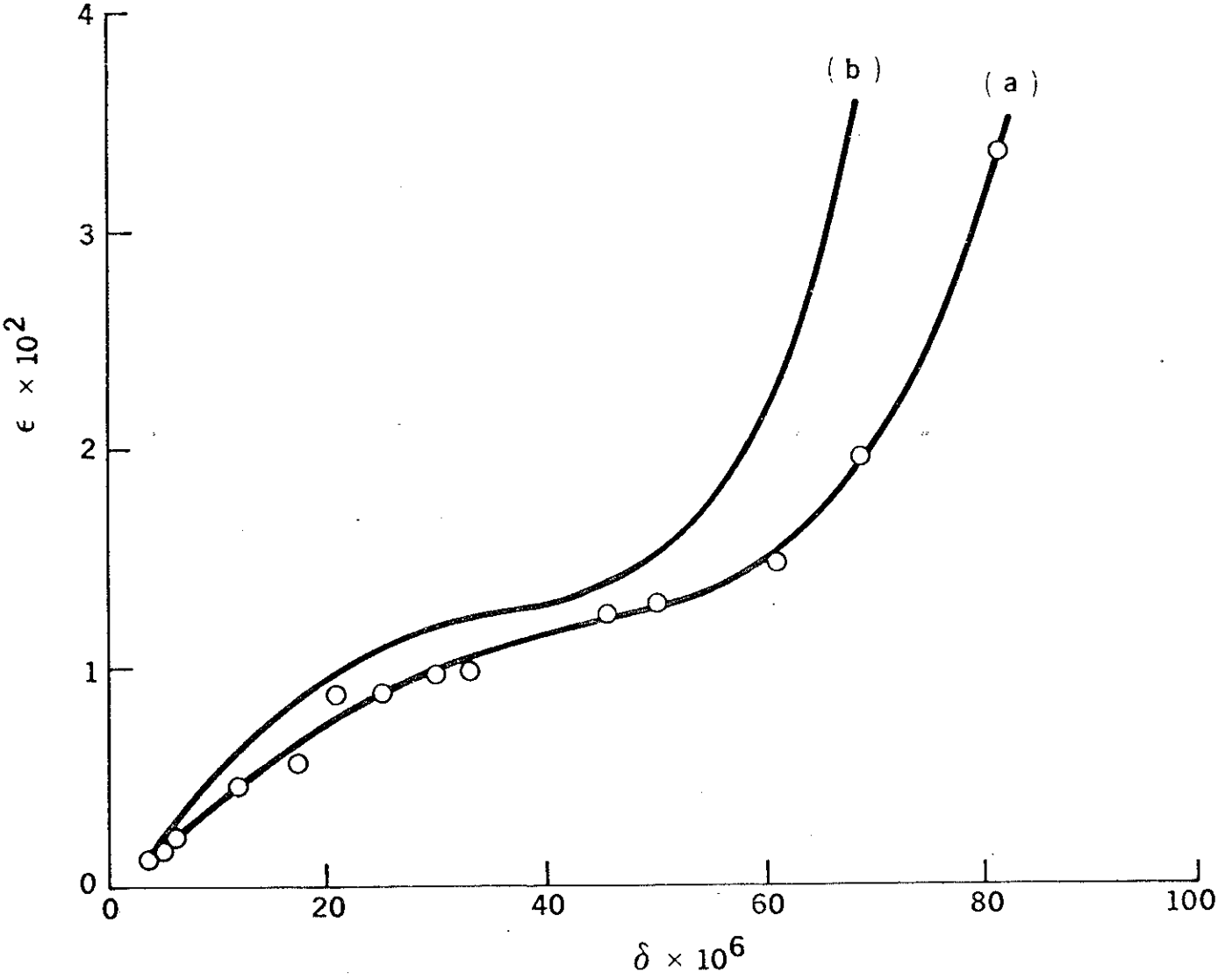

FIGURE 3 (a) OVERALL MEASURED DAMPING PLOTTED AGAINST STRAIN OF THE OUTER LAYERS OF THE SPECIMENS. (b) REAL INTERNAL FRICTION PLOTTED AGAINST STRAIN

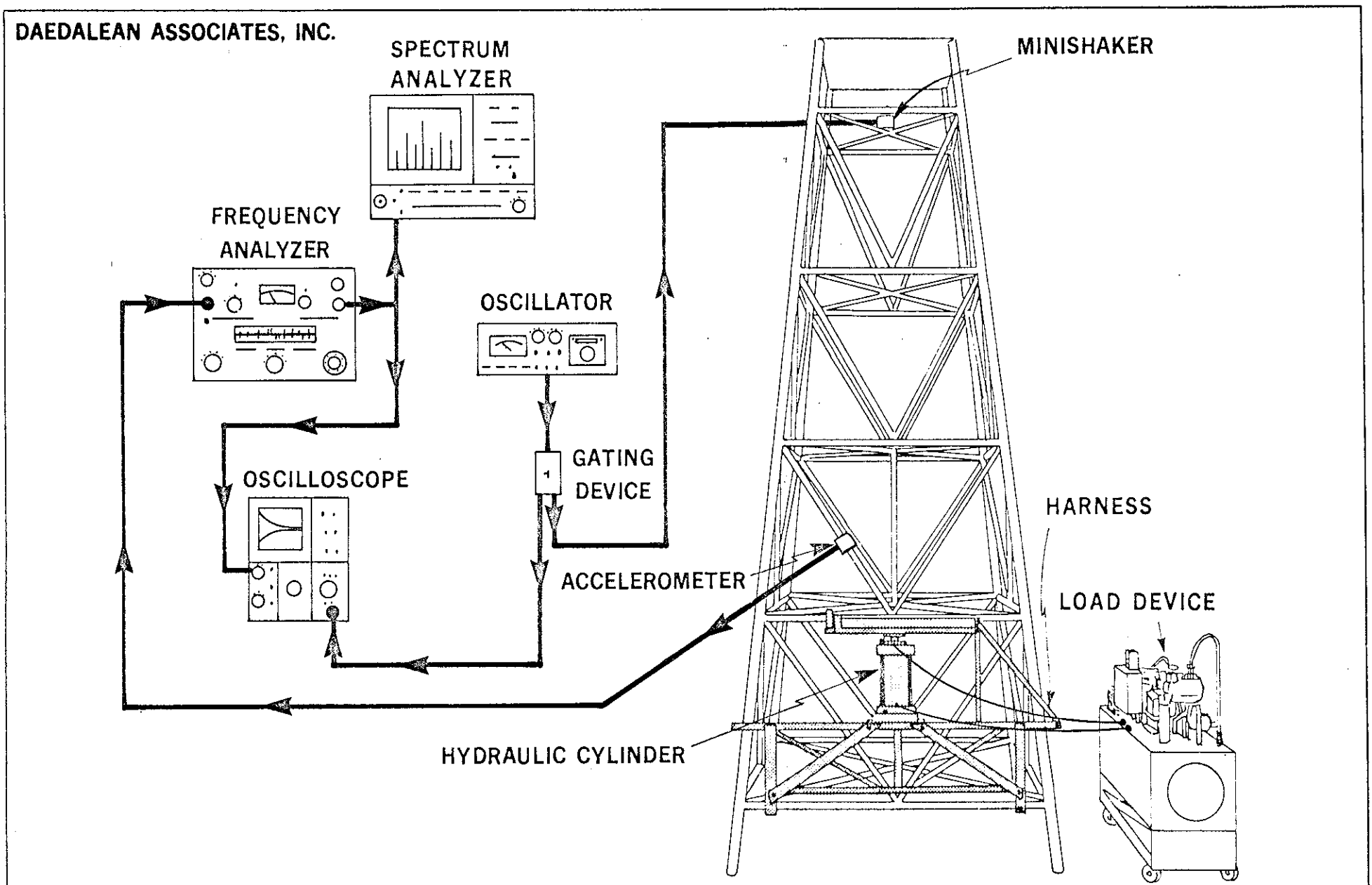

FIGURE 4 SCHEMATIC REPRESENTATION OF THE EQUIPMENT USED IN APPLYING THE IFD/NDE TECHNIQUE TO THE 1/14 SCALE MODEL OFFSHORE STRUCTURE INCLUDING THE TEST EQUIPMENT, THE LOADING DEVICE AND HARNESS, AND THE MODEL STRUCTURE

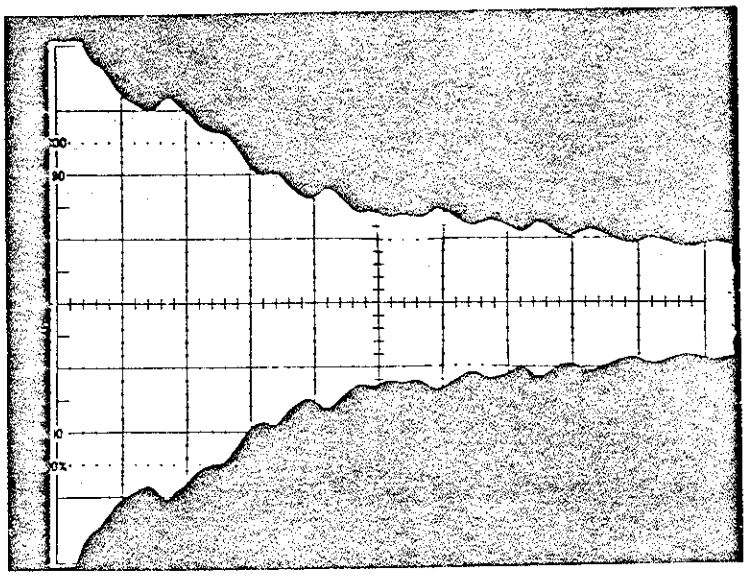

DECAY CURVE PRIOR TO FAILURE INCEPTION

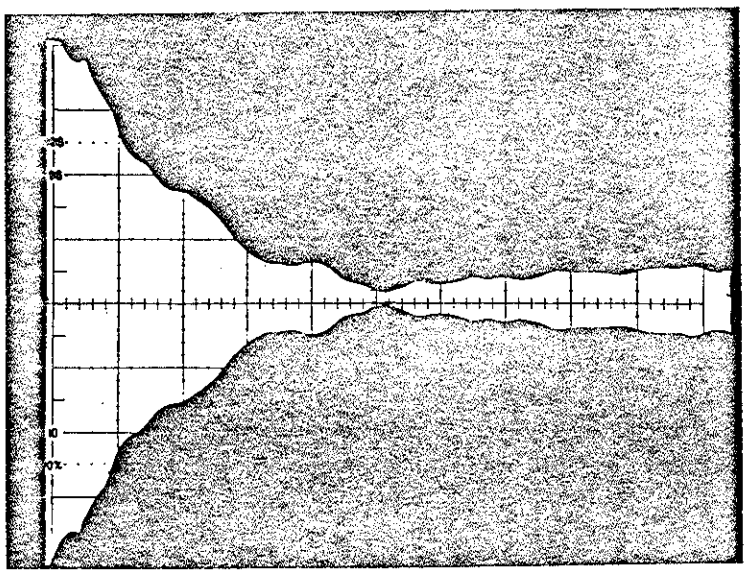

DECAY CURVE FOLLOWING FAILURE INCEPTION

FIGURE 5 REPRESENTATIVE DECAY CURVES PRIOR TO AND AFTER MEMBER FAILURE INCEPTION

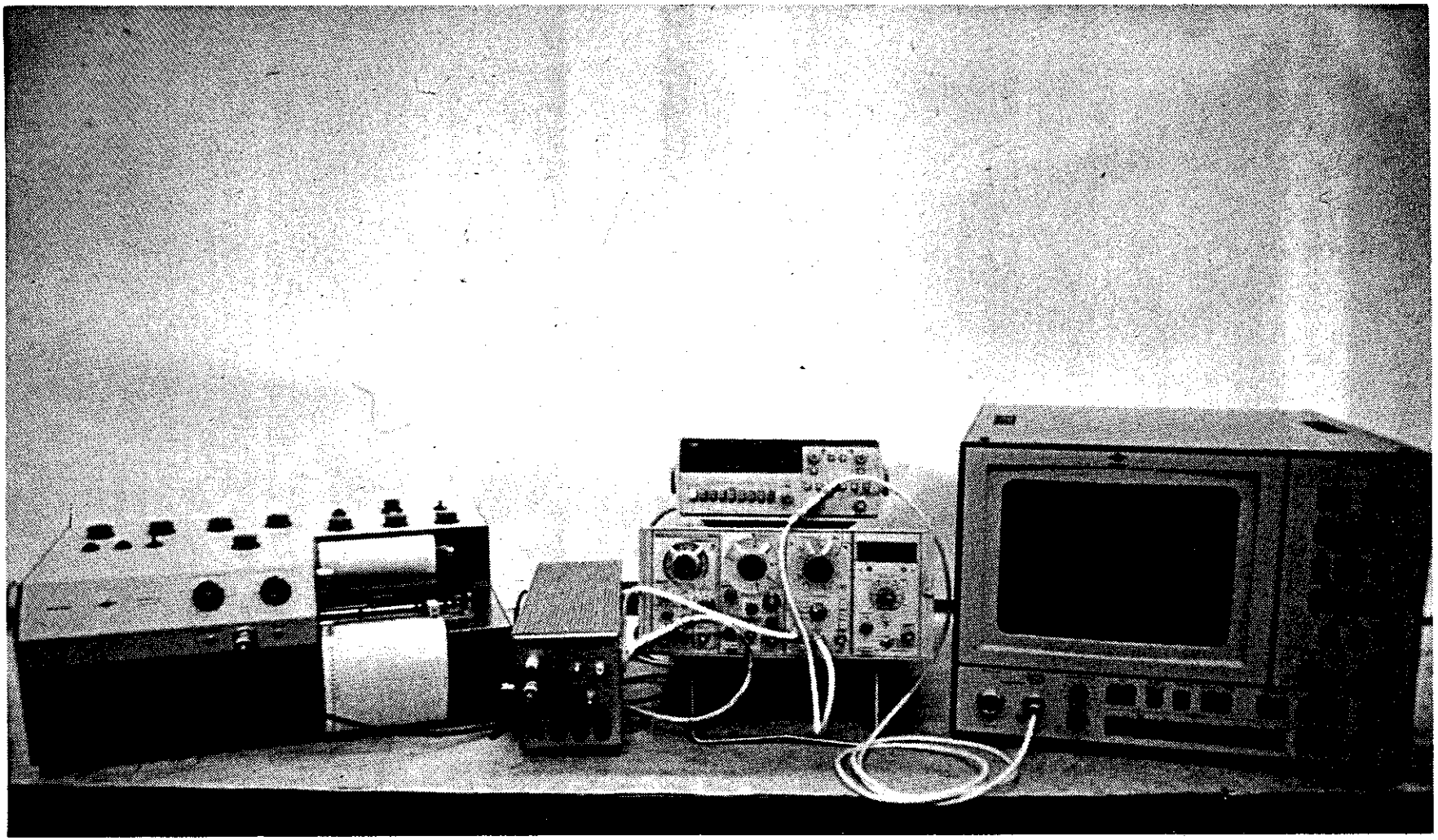

FIGURE 6 ELECTRONIC EQUIPMENT USED FOR IFD ANALYSIS OF MODEL OFFSHORE STRUCTURE

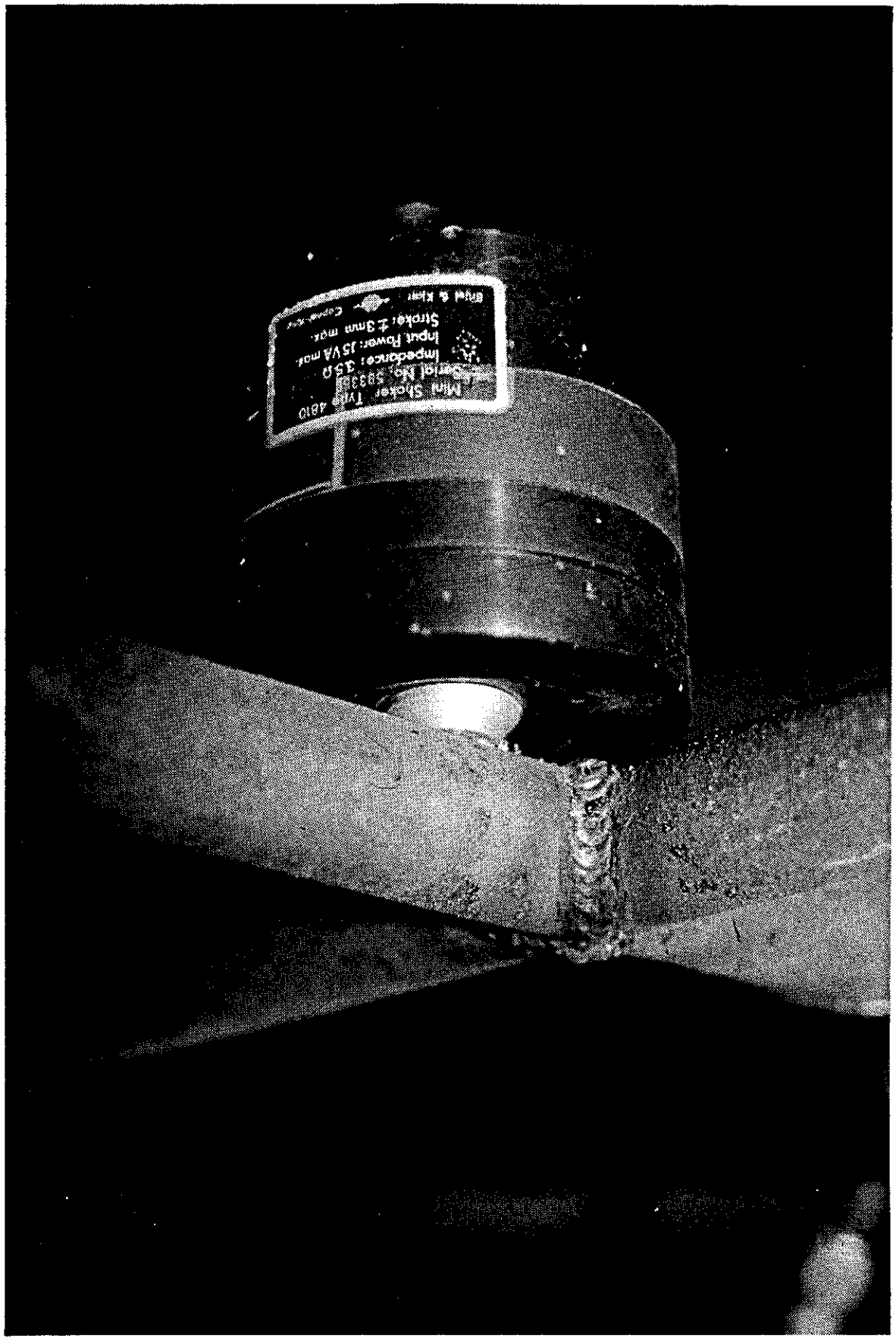

FIGURE 7 INPUT TRANSDUCER (MINI-SHAKER) MOUNTED IN A TOP CENTRAL LOCATION

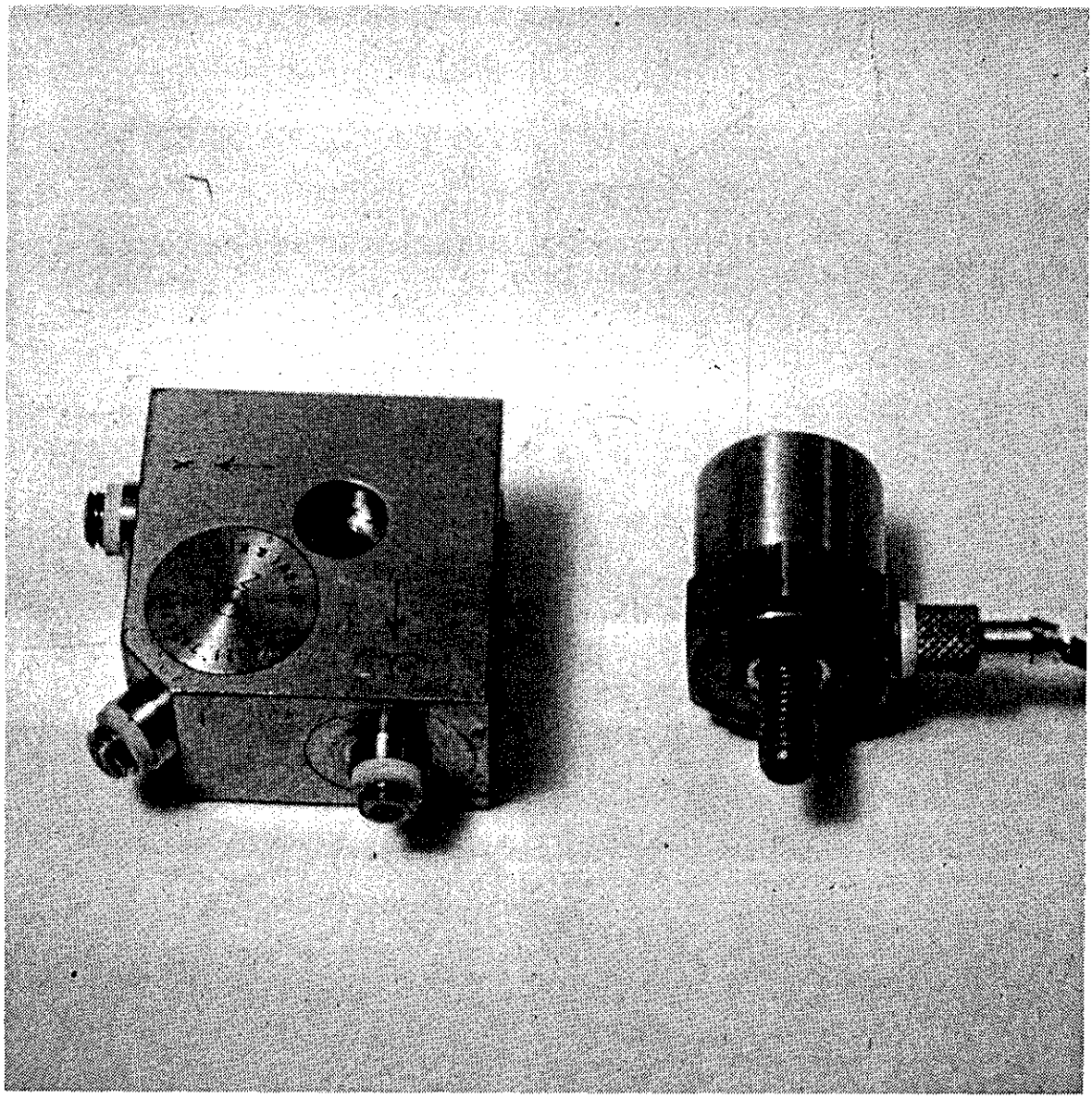

FIGURE 8 ONE DIMENSIONAL AND THREE DIMENSIONAL ACCELEROMETERS USED TO MONITOR MODEL OFFSHORE STRUCTURE

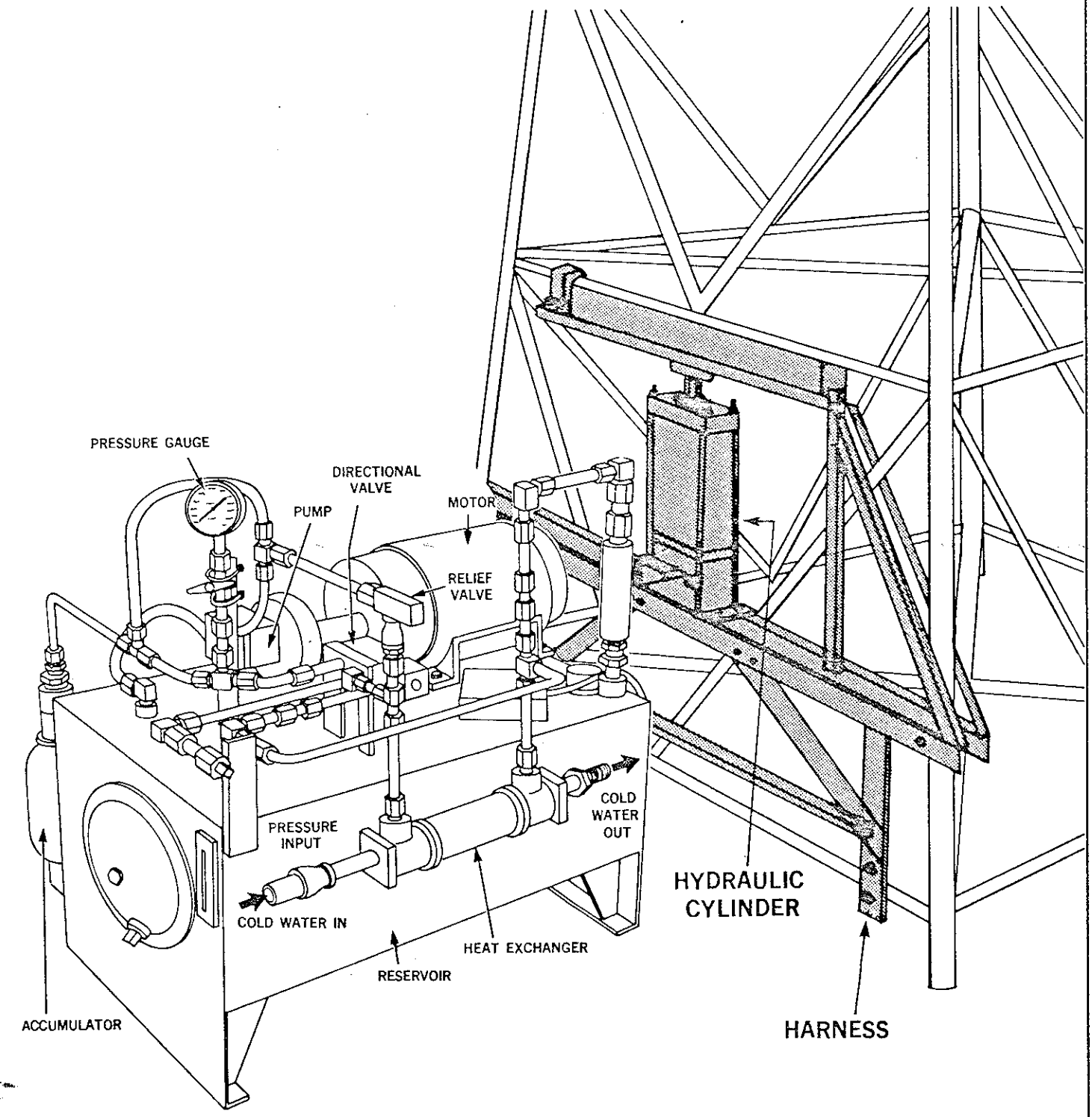

FIGURE 9 ILLUSTRATION OF THE ELECTROHYDRAULIC LOADING APPARATUS INCLUDING THE LOAD TRANSFER HARNESS

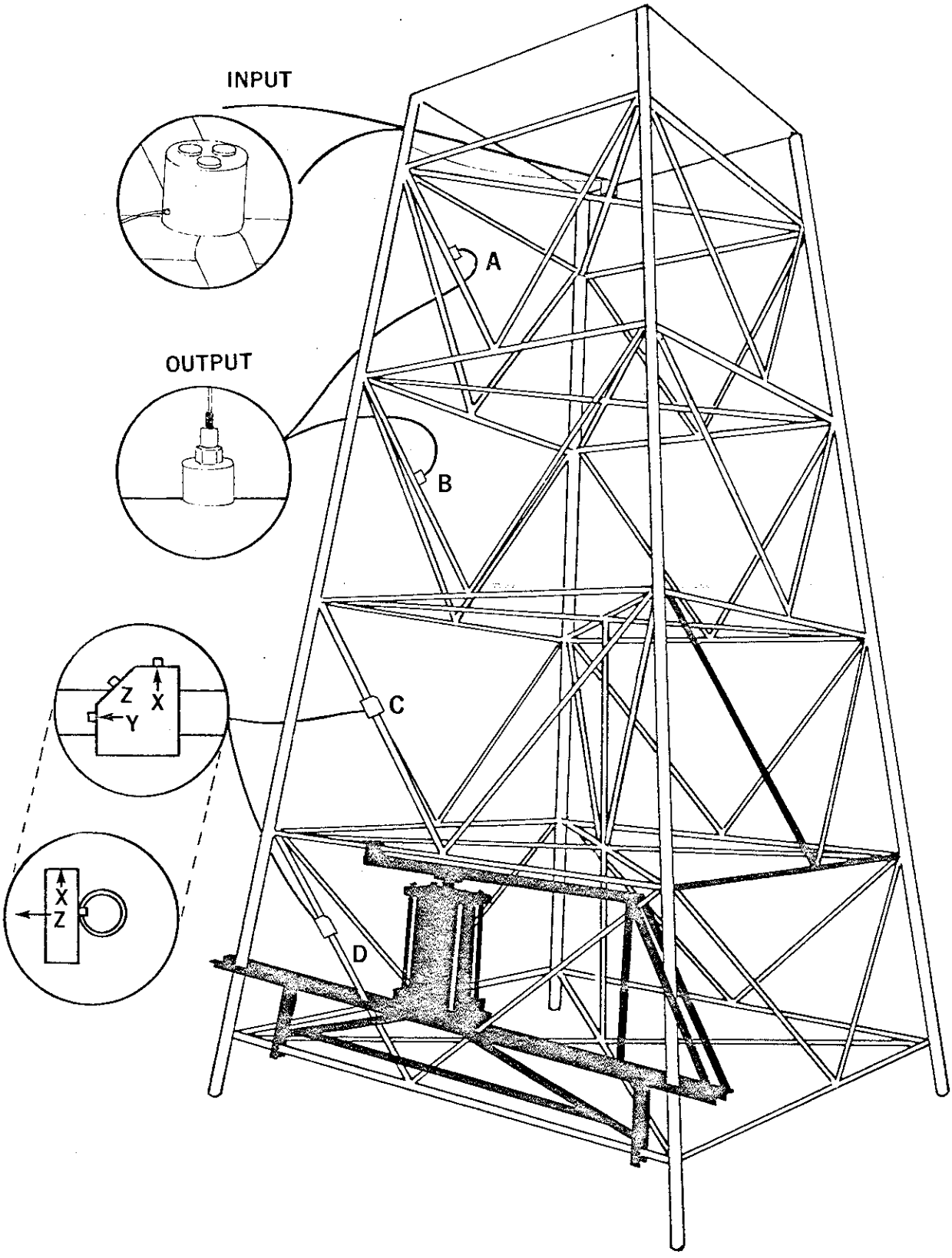

FIGURE 10 ACCELEROMETER LOCATIONS FOR ANALYSIS OF CRACK DETECTION

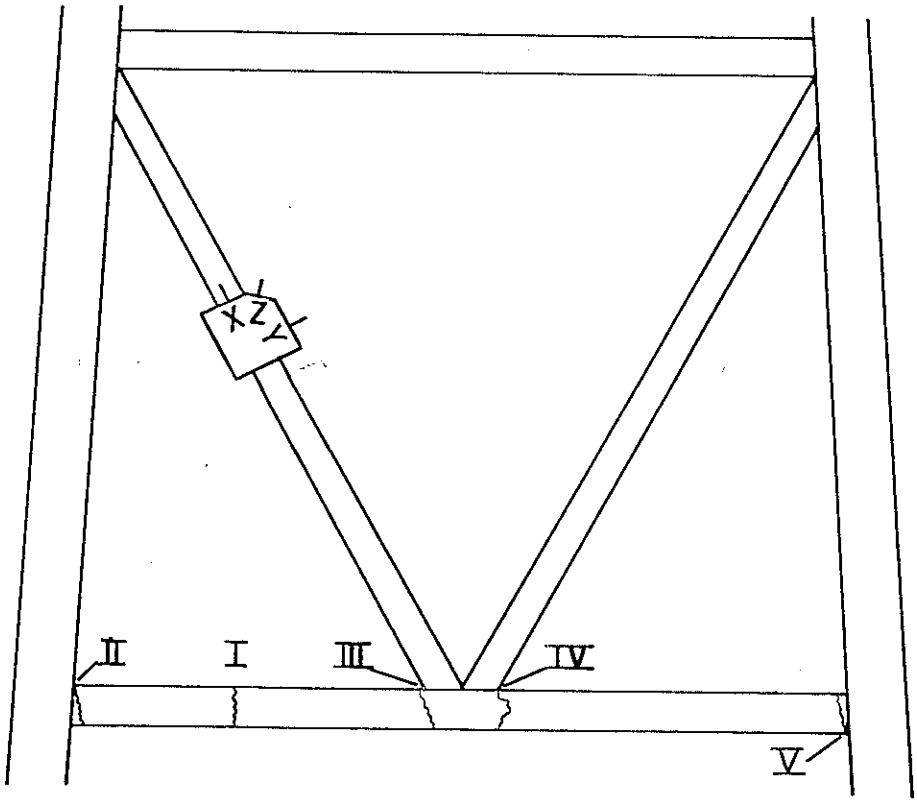

FIGURE 11 LOCATION OF WELD JOINTS (II - V) AND TEST NOTCHES (I - V) ON MODEL TOWER STRUCTURE

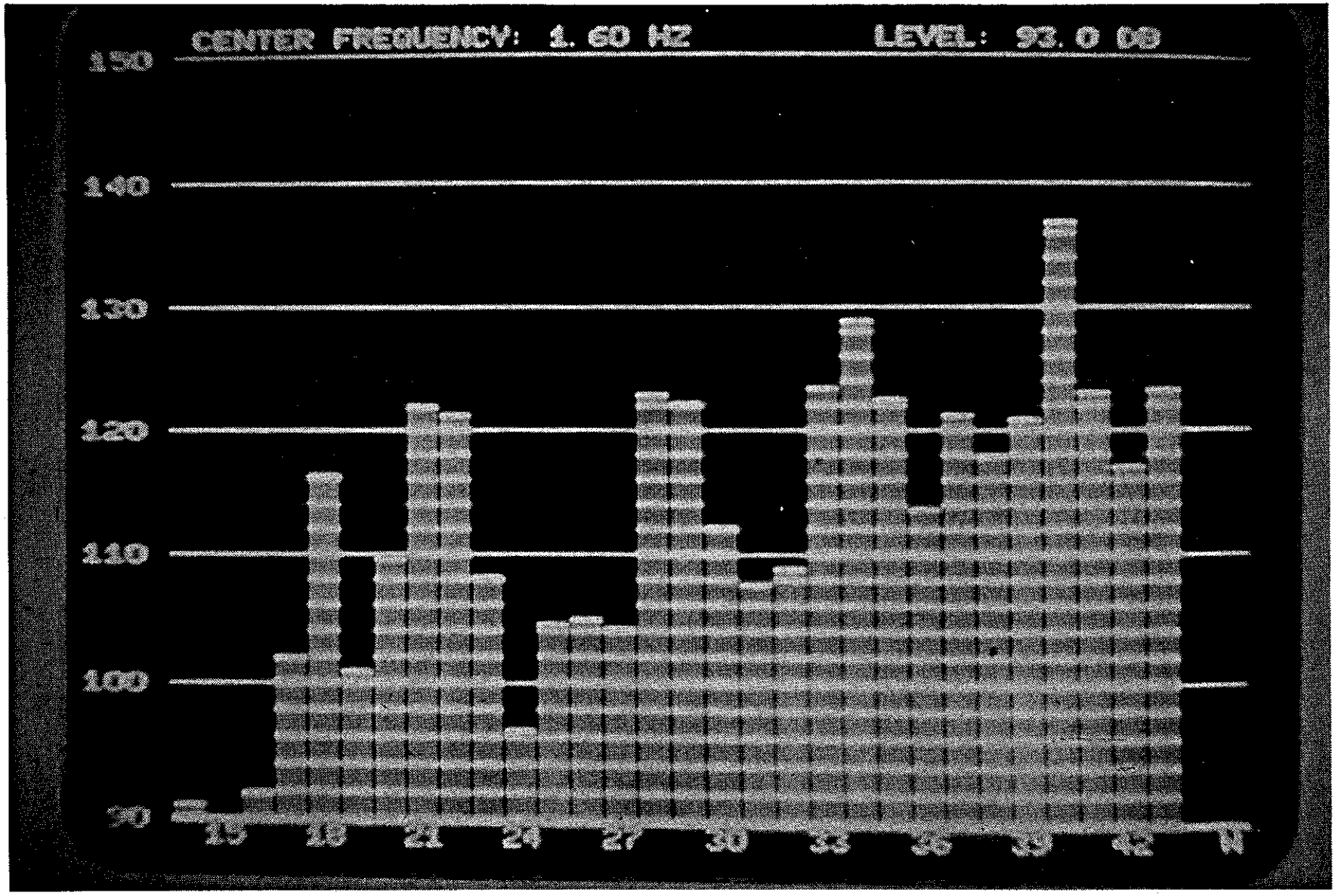

FIGURE 12 REPRESENTATIVE FREQUENCY SPECTRUM OF THE MODEL OFFSHORE STRUCTURE DISPLAYED ON REAL TIME SPECTRUM ANALYZER

DAEDALEAN ASSOCIATES, Inc.

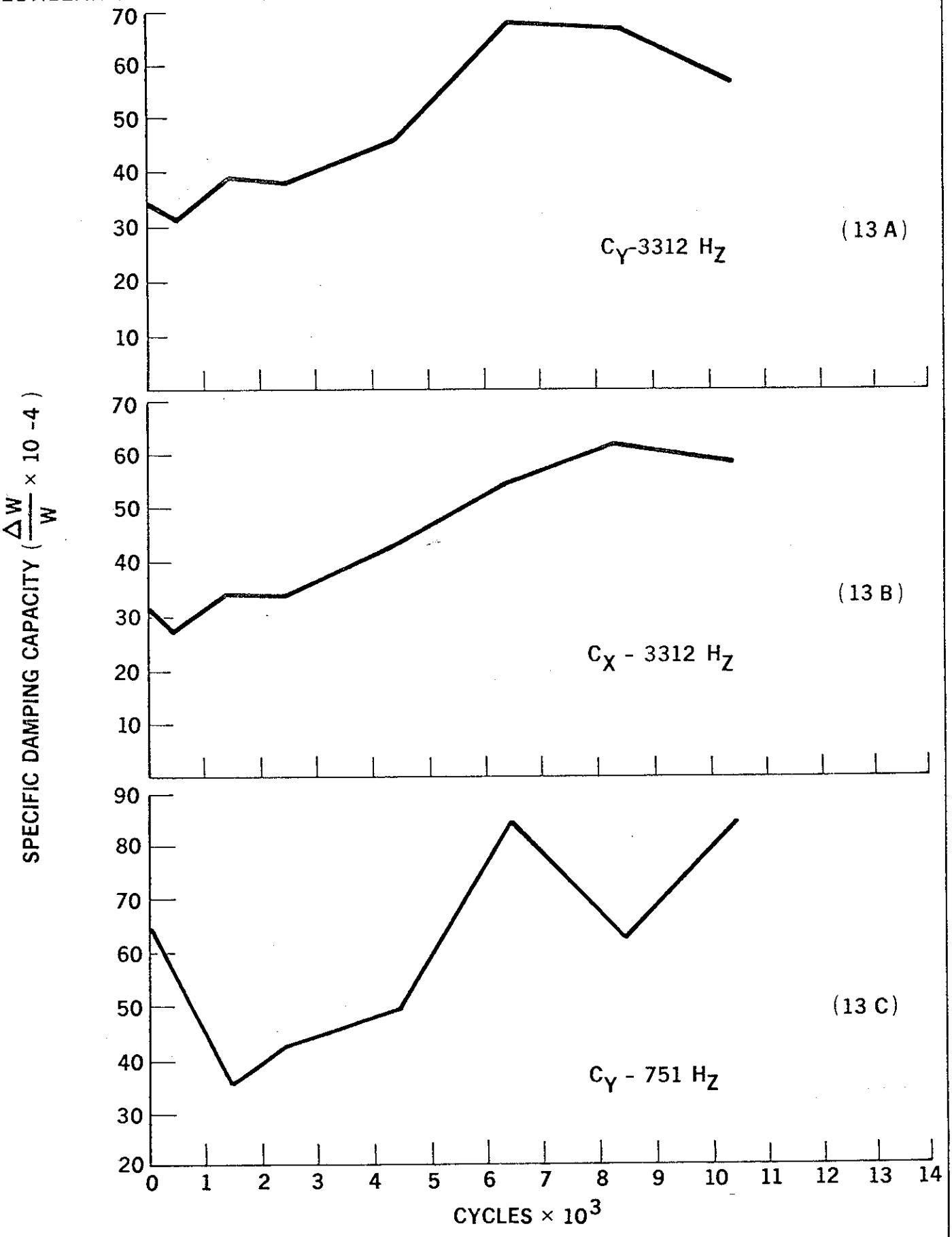

FIGURE 13 SPECIFIC DAMPING CAPACITY VERSUS CYCLES (FATIGUE TEST-2)

ACCELEROMETER C Z AXIS 2740 HZ

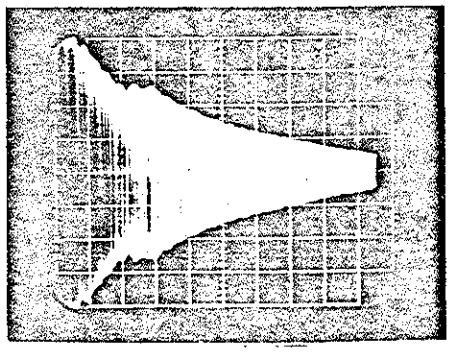

BASELINE

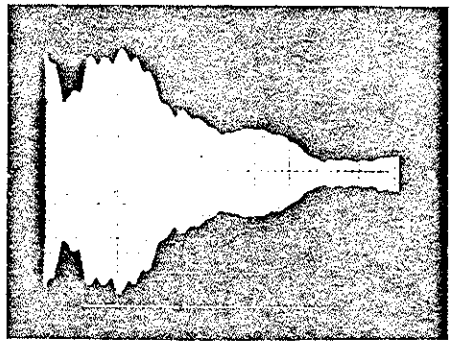

CRACK AT WELD III

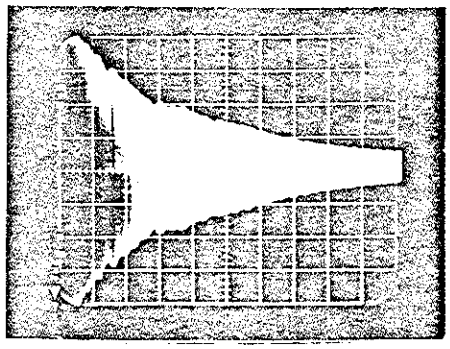

5,000 CYCLES

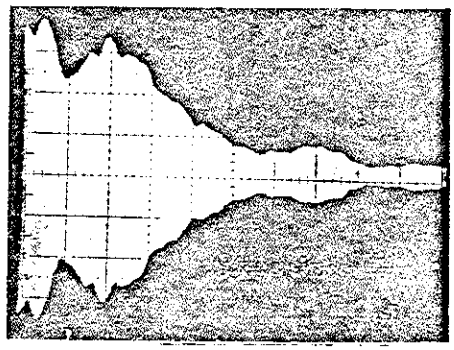

BREAK AT WELD III

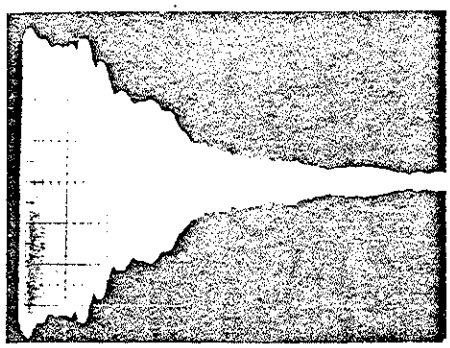

CRACK AT WELD II

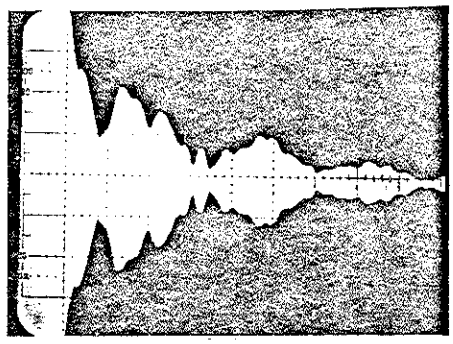

CRACK AT WELD IV

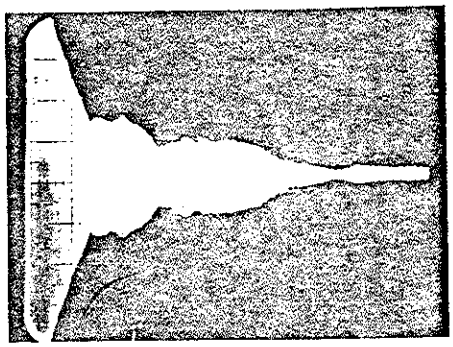

BREAK AT WELD II

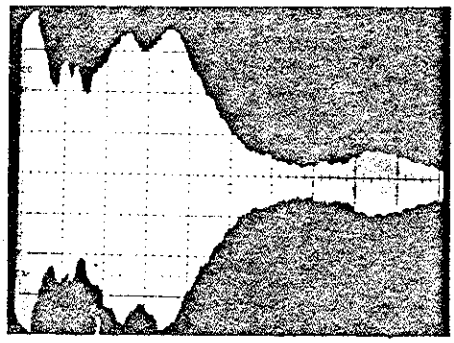

BREAK AT WELD IV

FIGURE 14 REPRESENTATIVE DECAY CURVES OF THE 1/14 SCALE MODEL OFFSHORE STRUCTURE FATIGUE FAILURE TESTS

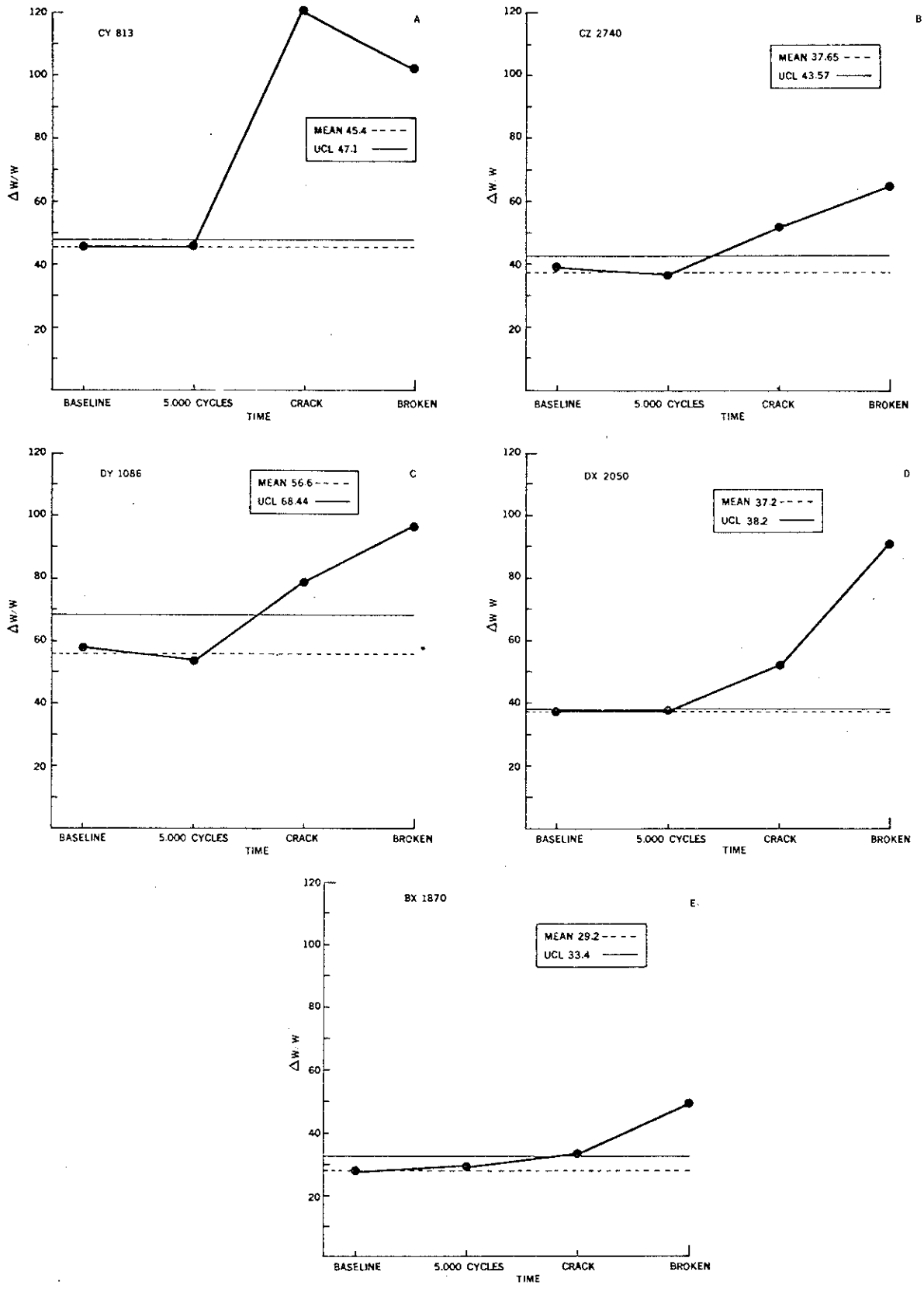

FIGURE 15 SPECIFIC DAMPING CAPACITY VERSUS TIME USING 99% UPPER CONFIDENCE LIMIT IN DETECTING INCIPIENT CRACKING IN THE 1/14 SCALE MODEL OFFSHORE STRUCTURE (FATIGUE TEST-3)

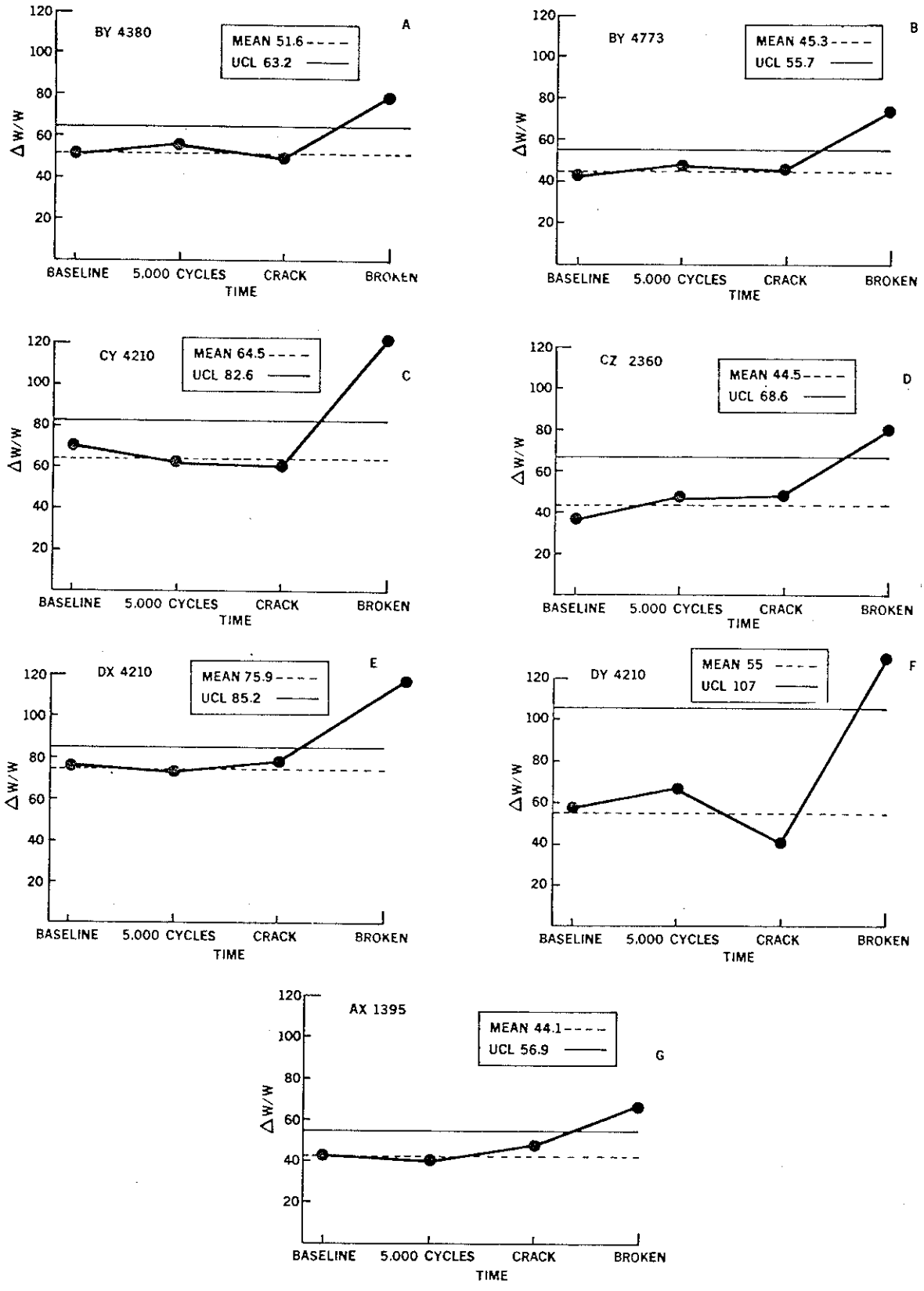

FIGURE 16 SPECIFIC DAMPING CAPACITY VERSUS TIME USING 99% UPPER CONFIDENCE LIMIT IN DETECTING MEMBER FAILURE IN THE 1/14 SCALE MODEL OFFSHORE STRUCTURE (FATIGUE TEST-3)

APPENDIX A

A.0 ANALYSIS OF NDE RESPONSES

A.1 Data Analysis Technique

The measured values of the specific damping capacity are used in a point by point determination of the base line equation for synthetic rope specimens. Each data point consists of a finite number of measurements (five for this data program) taken on the instant photograph. These data points are converted to a single specific damping capacity number by statistical averaging and analytical methods. The statistical averaging method performed on the numerous measurements taken from the output decay enables the average specific damping capacity value to be calculated from the "least squares linear curve fit." The statistical methods used to calculate the specific damping capacity are predicated upon the definition of elements that combine to provide analytically the existence of the "best" fit of a line through the measurements taken from the output decay. The confidence limit (defined as a function of the standard deviation of the set of measurements) is a measure of the logarithmic decay. The elements that are utilized for the determination of the specific damping capacity are defined in the following sections. The standard error of estimate (Section A.4) and the confidence limits (Section A.5) are included to

identify the analysis for the data scatter under cyclic loading fatigue conditions. Section A.6 addresses the analytical method used to determine the effect of different operators on the specific damping capacity measurements. Section A.7 is the software program for data reduction and generation of the specific damping capacity value.

A.1.1 Mean of a Sample

The arithmetic mean, $\bar{x}$, of a sample set containing n pieces of data is:

$$\bar{x} = \frac{1}{n} \sum_{i=1}^{n} x_i \qquad [A-1]$$

The arithmetic mean (denoted "mean") is assumed to be a stable average, not unduly affected by moderately large or small data points.

A.1.2 Variance of a Sample

The variance, s^2, of a sample set containing n pieces of data, with sample mean, $\bar{x}$, is:

$$s^2 = \frac{1}{n} \left[\sum_{i=1}^{n} (x^2_i) - n \bar{x}^2 \right] \qquad [A-2]$$

The variance is the minimum of the sum of the squares of the deviations taken with respect to the mean, and is a measure of the dispersion of the data about the sample mean.

A.1.3 Least-Squares Curve Fit

The linear least-squares fit of input data points (x_i, y_i) is calculated using the following:

$$\text{Slope} = m = \frac{\dfrac{\sum_{i=1}^{n} x_i \sum_{i=1}^{n} y_i}{n} - \sum_{i=1}^{n} x_i y_i}{\dfrac{\left(\sum_{i=1}^{n} x_i\right)^2}{n} - \sum_{i=1}^{n} x_i^2}$$

and [A-3]

$$\text{Intercept} = b = \frac{\sum_{i=1}^{n} y_i - m \sum_{i=1}^{n} x_i}{n}$$

where y_i is the measured specific damping $\frac{\Delta W}{W}$ and x_i is the corresponding number of load cycles (LC_n). The estimated value of specific damping $\left[\frac{\Delta W}{W}\right]_{est}$ is found by solving the equation:

$$\left[\frac{\Delta W}{W}\right]_{est} \equiv y_{est} = mx + b \qquad [A-4]$$

The correlation coefficient (r^2) is the fraction of the total variation which is explained by the least-squares regression line or how well the least-squares regression line fits the sample data, i.e.,

$$r^2 = \frac{\text{Explained Variation}}{\text{Total Variation}} \qquad [A-5]$$

The correlation coefficient can be computed from:

$$r^2 = m \left[\frac{\sum_{i=1}^{n} x_i \sum_{i=1}^{n} y_i}{n} - \sum_{i=1}^{n} x_i y_i \right] \Bigg/ \left[\sum_{i=1}^{n} y_i^2 - \frac{\left(\sum_{i=1}^{n} y_i \right)^2}{n} \right] \qquad [A-6]$$

In practice, r^2, lies between 0 and 1.

A.1.4 Standard Error of Estimate

A measure of the scatter about the regression curve, $y_{est} = f(x)$ is:

$$S_{y \cdot x} = \left[\frac{1}{n} \left(\sum_{i=1}^{n} (y_i)^2 - b \sum_{i=1}^{n} y_i - m \sum_{i=1}^{n} x_i \, y_i \right) \right]^{\frac{1}{2}} \quad [A-7]$$

which is the standard error of estimate of y on x.

A.1.5 Confidence Limits

The estimated value of the sample y at a corresponding $x - x_o$ is $y_{est} = f(x_o)$. At a specified probability level, σ, a degree of confidence for the estimated parameter can be calculated. An estimate of the interval in which the estimate of the sample value y will be found at the specified probability level is given by:

$$y_p = y_{est} \pm \left[\frac{t. \, S_{y-x}}{(n-2)^{\frac{1}{2}}} \right] \left[n + 1 + \left(\frac{n(x_o - \bar{x})^2}{S_x^{\,2}} \right) \right]^{\frac{1}{2}} \quad [A-8]$$

where t is the Student's statistic with n-2 degrees of freedom (df). The value of the t statistic can be found in tables. The estimated values define the confidence limits of the dependent variable at the specified probability level.

A.1.6 Operator Significance

The possibility of using data obtained by two operators exists providing the differences between the two sets of data

can be proven nonsignificant. This can be accomplished by determining whether the correlation coefficient r and r_2, drawn from samples n and n_2, differ significantly from each other.

To prove the differences nonsignificant, a null hypothesis (H_o:) is formulated that any observed differences are due to chance fluctuations in two operators sampling from the same population. The null hypothesis is:

$$H_o: \quad (\mu_{z_1} \neq \mu_{z_2}) \qquad [A-9]$$

i.e., there is no significant difference between the two sample means. The alternate hypothesis is:

$$H_1: \quad (\mu_{z_1} \neq \mu_{z_2}) \qquad [A-10]$$

i.e., the difference between the two sample means is significant.

To test the null hypothesis, use is made of Fisher's Z transformation given by:

$$Z = \frac{1}{2} \ln \frac{1 + r}{1 - r} \qquad [A-11]$$

the statistic, z, given by:

$$z = \frac{Z_1 - Z_2 - \mu_{z_1 - z_2}}{\sigma_{z_1 - z_2}} \qquad [A-12]$$

is calculated and used in a two-tailed test to determine whether the value falls within the region of nonsignificance at the specified probability level. Z_1 and Z_2 are calculated for corresponding values of r and r^2. In the equation for z, (B-12),

$$\sigma_{z_1 - z_2} = \left[\frac{1}{n_1 - 3} + \frac{1}{n_2 - 3} \right]^{\frac{1}{2}} \qquad [A-13]$$

and

$$\mu_{z_1 - z_2} = \mu_{z_1} - \mu_{z_2} \qquad [A-14]$$

The null hypothesis, H_o:, is accepted if A lies within the critical region specified by the preassigned probability level; i.e., the observed differences in the data are not significant at the specified probability level. If, however, z lies outside the critical region, then reject H_o: and accept H_1:; i.e., the observed differences in the data are significant at the specified probability level.

A.2 Software Program Listing

```
FORTRAN IV      V02.1-1     Tue 04-Sep-79 09:47:41          PAGE 001

0001            LOGICAL*1 ICAR,YES
0002            DATA YES/'Y'/
0003            REAL N,NN
0004            DIMENSION ALPHA(10),A(10)
0005            PRINT 1
0006  1         FORMAT('-')
0007            TYPE 2
0008  2         FORMAT(' INPUT ID INFO, PRECEDED BY A BLANK SPACE')
0009            ACCEPT 3
0010  3         FORMAT(' THIS WILL BE REPLACED WITH ID  ')
0011            PRINT 3
0012            PRINT 4
0013  4         FORMAT(' ','ALPHA',T10,'STD DEV   ^W/W',T27,
                1'N/DIVISION  A0    A1    A2    A3    A4    A5')
0014            PRINT 5
0015  5         FORMAT('   *E-4',T12,'*E-4    *E-4     CYCLES')
0016  6         SMEAN=0.0
0017            SDEVA=0.0
0018            SUM=0.0
0019            TYPE 10
0020  10        FORMAT(' PLEASE INPUT THE N/DIVISION AND A0',
                1'EACH FOLLOWED BY <CR>')
0021            ACCEPT 20,N,A0
0022  20        FORMAT(F6.1)
0023            TYPE 30
0024  30        FORMAT(' INPUT A1 THRU AN ONE AT A TIME FOLLOWED BY <CR> ?')
0025            TYPE 32
0026  32        FORMAT(' INPUT 0. AS THE LAST AN')
0027            I=1
0028  35        ACCEPT 40,A(I)
0029  40        FORMAT(F5.1)
0030            IF(A(I).EQ.0.0)GO TO 60
0032            NN=N*I
0033            ALPHA(I)=(1./NN)*(ALOG(A0/A(I)))
0034            SUM=SUM+ALPHA(I)
0035            I=I+1
0036            GO TO 35
0037  60        I=I-1
0038            AVG=SUM/I
0039            DO 70 J=1,I
0040            SDEVA=SDEVA+(AVG-ALPHA(J))**2
0041  70        CONTINUE
0042            SDEV=SQRT(SDEVA/I)*10000
0043            DELTAW=1-EXP(-2*AVG)
0044            DELTAW=DELTAW*10000
0045            AVG=AVG*10000
```

```
0046          PRINT 80,AVG,SDEV,DELTAW,N,A0,(A(J),J=1,5)
0047   80     FORMAT(' ',F6.2,T10,F5.2,T17,F8.2,T30,F6.1,T38,6(F5.1))
0048          TYPE 90
0049   90     FORMAT(' ARE YOU DONE ? ')
0050          ACCEPT 95,ICAR
0051   95     FORMAT(A1)
0052          IF(ICAR.EQ.YES)GO TO 100
0054          GO TO 6
0055   100    STOP
0056          END
FORTRAN IV       Storage Map for Program Unit .MAIN.

Local Variables, .PSECT $DATA, Size = 000224 (   74. words)

Name   Type  Offset     Name   Type  Offset     Name   Type  Offset
AVG    R*4   000162     A0     R*4   000154     DELTAW R*4   000174
I      I*2   000160     ICAR   L*1   000126     J      I*2   000166
N      R*4   000130     NN     R*4   000134     SDEV   R*4   000170
SDEVA  R*4   000144     SMEAN  R*4   000140     SUM    R*4   000150
YES    L*1   000120

Local and COMMON Arrays:

Name     Type   Section Offset  ------Size------ Dimensions
A        R*4    $DATA   000050  000050 (   20.) (10)
ALPHA    R*4    $DATA   000000  000050 (   20.) (10)

Subroutines, Functions, Statement and Processor-Defined Functions:

Name   Type   Name   Type   Name   Type   Name   Type   Name   Type
ALOG    R*4   EXP     R*4   SQRT    R*4

FORTRAN IV      V02.1-1     Thu 10-May-79 09:46:44              PAGE 001

0001          DIMENSION AS(100),ALF(100)
0002          LOGICAL*1 ICAR,YES
0003          DATA YES/'Y'/
0004   5      X=0
0005          Y=0
0006          N=1
0007          TYPE 10
0008   10     FORMAT(' INPUT UP TO 100 VALUES, EACH FOLLOWED BY <CR>')
0009          TYPE 12
0010   12     FORMAT(' INPUT 0. <CR> AFTER LAST VALUE')
0011   15     ACCEPT 20,ALF(N)
0012   20     FORMAT(F5.2)
0013          X=X+ALF(N)
0014          AS(N)=ALF(N)**2
0015          Y=Y+AS(N)
0016          IF(ALF(N).EQ.0.0) GO TO 30
0018          N=N+1
```

```
0019          GO TO 15
0020    30    N=N-1
0021          PRINT 40
0022    40    FORMAT('0','MEAN',5X,'STD DEV',5X,'C LEV',5X,'UCL')
0023          ALPHAM=X/N
0024          STDEV=SQRT(ABS((Y-(N*ALPHAM**2))/N))
0025          PRINT 50,ALPHAM,STDEV
0026    50    FORMAT(' ',F5.2,5X,F5.3,5X)
0027    55    TYPE 60
0028    60    FORMAT(' WHAT LEVEL OF CONFIDENCE?')
0029          ACCEPT 70,CON
0030    70    FORMAT(F4.2)
0031          TYPE 80
0032    80    FORMAT(' INPUT T-STATISTIC')
0033          ACCEPT 90,TSTAT
0034    90    FORMAT(F5.3)
0035          UCL=STDEV*TSTAT+ALPHAM
0036          TYPE 95,ALPHAM,STDEV,CON,TSTAT,UCL
0037    95    FORMAT(' MEAN=',F5.2,' STDEV=',F5.3,' CONF LEV=',F5.2,
             1' TSTAT=',F5.3,' UCL=',F5.2)
0038          PRINT 100,CON,UCL
0039    100   FORMAT(' ',T22,F5.2,5X,F5.2)
0040          TYPE 110
0041    110   FORMAT(' ANY MORE CONFIDENCE LEVELS FOR THIS DATA?')
0042          ACCEPT 120,ICAR
0043    120   FORMAT(A1)
0044          IF(ICAR.NE.YES)GO TO 130
0046          GO TO 55
0047    130   TYPE 140
0048    140   FORMAT(' DO YOU WANT A LIST OF VALUES?')
0049          ACCEPT 150,ICAR
0050    150   FORMAT(A1)
0051          IF(ICAR.NE.YES)GO TO 160
0053          PRINT 155,(ALF(J),J=1,N)
0054    155   FORMAT(' ',F5.2)
0055    160   TYPE 170
0056    170   FORMAT(' ANY MORE DATA TO ANALYZE?')
FORTRAN IV      V02.1-1     Thu 10-May-79 09:46:44                    PAGE 002

0057          ACCEPT 180,ICAR
0058    180   FORMAT(A1)
0059          IF(ICAR.EQ.YES)GO TO 5
0061          STOP
0062          END
FORTRAN IV      Storage Map for Program Unit .MAIN.

Local Variables, .PSECT $DATA, Size = 001530 (  428. words)
```

Name	Type	Offset	Name	Type	Offset	Name	Type	Offset
ALPHAM	R*4	001460	CON	R*4	001470	ICAR	L*1	001444
J	I*2	001504	N	I*2	001456	STDEV	R*4	001464
TSTAT	R*4	001474	UCL	R*4	001500	X	R*4	001446
Y	R*4	001452	YES	L*1	001440			

Local and COMMON Arrays:

Name	Type	Section	Offset	------Size------	Dimensions
ALF	R*4	$DATA	000620	000620 (200.)	(100)
AS	R*4	$DATA	000000	000620 (200.)	(100)

Subroutines, Functions, Statement and Processor-Defined Functions:

Name	Type	Name	Type	Name	Type	Name	Type	Name	Type
ABS	R*4	SQRT	R*4						

APPENDIX B

B.0 CALCULATIONS OF BENDING LOADS FOR FATIGUE OF OFFSHORE STRUCTURE

Material: ASTM A53-B carbon steel pipe

Fy = 36,000 psi

Framing Members: 3/4 inch nominal diameter, Schedule 40,

Moment of Inertia about neutral axis:

$I = 0.037$ in.^{4}

Section Modulus: $S = 0.0071$ in.^{3}

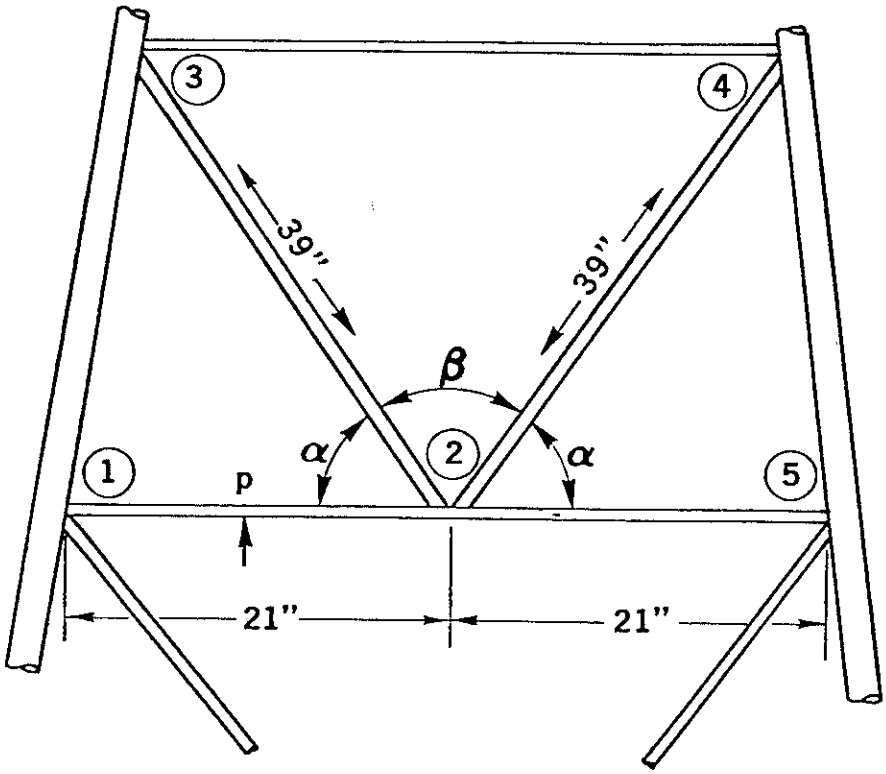

$\alpha = 60.524°$ $B = 58.952°$

B.1 Using Moment Distribution Method

Stiffness factors for members connected at Joint 2.

$$K = \frac{4EI}{l}$$

where:

E = modulus of elasticity

l = length of member

$$K_{12} = K_{25} = \frac{4EI}{29''} = 0.19EI$$

$$K_{23} = K_{24} = \frac{4EI}{39''} = 0.103EI$$

B.2 Distribution Factors

$$r_{12} = \frac{K_{12}}{\Sigma K} = \frac{0.19EI}{(2 \times 0.19EI) + (2 \times 0.103EI)} = \frac{0.19EI}{0.586EI}$$

$$r_{12} = r_{25} = 0.325$$

$$r_{23} = r_{24} = \frac{0.103EI}{0.586EI} = 0.175$$

Load P is applied midspan member 1-2. Fixed end moment:

$$FEM_{12} = \frac{P\ell}{8} = \frac{21P}{8} = 2.625P$$

B.3 Distribution of Moments at Joint 2

r_{21} (FEM_{12}) = 0.325 (2.625P) = 0.853P

r_{23} (FEM_{12}) = 0.175 (2.625P) = 0.459P

Carry-over Factors C = 0.5

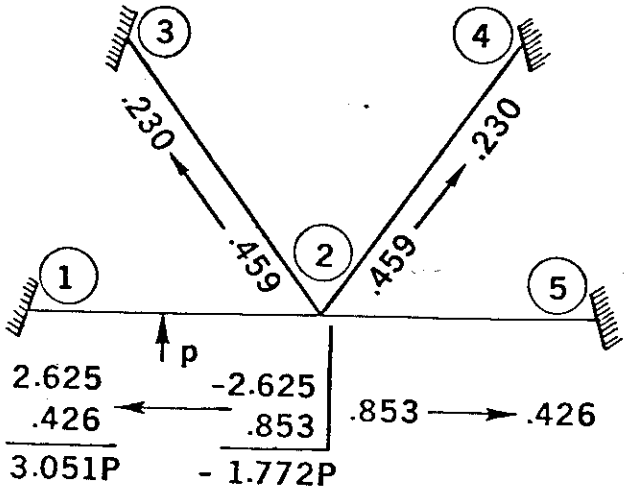

B.4 Results of Moment Distribution

M_{12} = 3.051 P

M_{21} = 1.772 P

These results were confirmed by slope-deflection technique calculations.

Moment Diagram:

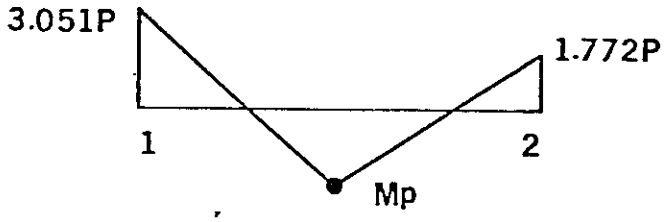

Moment at Point of Load:

$$M_p = \frac{3.051P + 1.772P}{2} - \frac{P\ell}{4}$$

$$M_p = 2.411P - 5.250P = 2.839P$$

B.5 Extreme Fiber Stress at Critical Points

$$f_b = \frac{M}{S}$$

at Joint 1 $f_b = \frac{3.051P}{0.071} = 42.97P$

at Joint 2 $f_b = \frac{1.772P}{0.071} = 24.96P$

at Point of Load $f_b = \frac{2.839P}{0.071} = 39.99P$

EXTREME FIBER STRESS	BENDING LOAD REQUIRED TO ACHIEVE DESIRED STRESS (POUNDS) MIDSPAN	JOINT 1
30% Fy = 10,800 psi	270	251
45% Fy = 16,200 psi	405	377
75% Fy = 27,000 psi	675	628

SECURITY CLASSIFICATION OF THIS PAGE (When Data Entered)

REPORT DOCUMENTATION PAGE

READ INSTRUCTIONS BEFORE COMPLETING FORM

1. REPORT NUMBER

2. GOVT ACCESSION NO.

3. RECIPIENT'S CATALOG NUMBER

4. TITLE (and Subtitle)
TECHNICAL REPORT ON THE LABORATORY APPLICATION OF A NONDESTRUCTIVE EVALUATION TECHNIQUE FOR DETECTING INCIPIENT CRACK FORMATION IN MODEL OFFSHORE STRUCTURES

5. TYPE OF REPORT & PERIOD COVERED
TECHNICAL PHASE REPORT

6. PERFORMING ORG. REPORT NUMBER

7. AUTHOR(s)
RAY G. BRASFIELD
DAVID C. FRESCH
BRUCE JACHOWSKI

8. CONTRACT OR GRANT NUMBER(s)
N00014-77-C-0567

9. PERFORMING ORGANIZATION NAME AND ADDRESS
DAEDALEAN ASSOCIATES, INC.
15110 FREDERICK ROAD
WOODBINE, MARYLAND 21797

10. PROGRAM ELEMENT, PROJECT, TASK AREA & WORK UNIT NUMBERS

11. CONTROLLING OFFICE NAME AND ADDRESS
OFFICE OF NAVAL RESEARCH
DEPARTMENT OF THE NAVY
800 N. QUINCY STREET
ARLINGTON, VIRGINIA 22217

12. REPORT DATE
MAY 1980

13. NUMBER OF PAGES

14. MONITORING AGENCY NAME & ADDRESS (If different from Controlling Office)
DEFENSE CONTRACT ADMINISTRATION SERVICES
MANAGEMENT AREA - BALTIMORE
300 E. JOPPA ROAD, HAMPTON PLAZA BLD. ROOM 200
TOWSON, MARYLAND 21204

15. SECURITY CLASS. (of this report)
UNCLASSIFIED

15a. DECLASSIFICATION DOWNGRADING SCHEDULE

16. DISTRIBUTION STATEMENT (of this Report)
DOCUMENT IS AVAILABLE TO THE PUBLIC THROUGH THE NATIONAL TECHNICAL INFORMATION SERVICE, SPRINGFIELD, VIRGINIA 22151.

17. DISTRIBUTION STATEMENT (of the abstract entered in Block 20, if different from Report)
SAME AS NUMBER 16

18. SUPPLEMENTARY NOTES

19. KEY WORDS (Continue on reverse side if necessary and identify by block number)
INTERNAL FRICTION DAMPING (IFD)
NONDESTRUCTIVE EVALUATION (NDE)
OFFSHORE TOWER
OFFSHORE STRUCTURE
CRACK DETECTION
MEMBER FAILURE
FREQUENCY SPECTRUM ANALYSIS

20. ABSTRACT (Continue on reverse side if necessary and identify by block number)
This report discusses the technical feasibility of applying an Internal Friction Damping - Nondestructive Evaluation technique for offshore structures. The theory of internal friction damping is presented as it has been historically applied to various materials. The report then discusses the methodology for the application of internal friction damping. The experimental apparatus and specific laboratory technique as applied to a 1/14 scale model offshore structure is next discussed in detail. The experimental test results are related to the feasibility of employing the test

DD FORM 1 JAN 73 1473 EDITION OF 1 NOV 65 IS OBSOLETE
S/N 0102-LF-014-6601

UNCLASSIFIED
SECURITY CLASSIFICATION OF THIS PAGE (When Data Entered)

technique as a device for detecting incipient cracking in offshore structures. The report includes discussion of specific conclusions and recommendations for further investigation of in-service offshore structures.